DP-MS-80-94 Rev. 1

SPECTRAL SCALES IN THE ATMOSPHERIC BOUNDARY LAYER

by

A. H. Weber
E. I. du Pont de Nemours & Co.
Savannah River Laboratory
Aiken, SC 29808

J. S. Irwin and W. B. Petersen
Meteorology and Assessment Division
Environmental Sciences Research Laboratory
Research Triangle Park, NC 27711

J. J. Mathis, Jr.
Environmental Field Measurements Branch
NASA Langley Research Center
Hampton, VA 23665

J. P. Kahler
U.S. Air Force
Headquarters Air Weather Service
Scott Air Force Base, IL 62225

Proposed for publication in the
Journal of Applied Meteorology

This paper was prepared in connection with work done under Contract No. DE-AC09-76SR00001 with the U.S. Department of Energy.

This document was prepared in conjunction with work accomplished under Contract No. DE-AC09-76SR00001 with the U.S. Department of Energy.

DISCLAIMER

ABSTRACT

Wind measurements from the Savannah River Laboratory — WJBF-TV tower in Beech Island, South Carolina were used to compute turbulence parameters which were then compared with similarity theory predictions summarized by Hanna (1981A). The parameters computed were standard deviations of the fluctuating velocity components σ_u, σ_v, and σ_w, and spectral scales λ_m and ℓ_E.

The correlation coefficients were highest for the standard deviations of the velocity components σ_u, σ_v, and σ_w. The averaged correlation coefficients for all three components were 0.60, 0.45, and 0.72 for unstable, stable, and neutral conditions, respectively.

The averaged correlation coefficient between computed and measured spectral maxima λ_{mu}, λ_{mv}, and λ_{mw}, were 0.66 for stable conditions and 0.65 for neutral conditions. Very low correlations of -0.11 and 0.01 were obtained for λ_{mu} and λ_{mv} in unstable conditions. The vertical wavelength λ_{mw}, however, had a correlation coefficient of 0.59 between measured and predicted values.

SPECTRAL SCALES IN THE ATMOSPHERIC BOUNDARY LAYER*

by

A. H. Weber
E. I. du Pont de Nemours & Co.
Savannah River Laboratory
Aiken, SC 29808

J. S. Irwin and W. B. Petersen*
Meteorology and Assessment Division
Environmental Sciences Research Laboratory
Research Triangle Park, NC 27711

J. J. Mathis, Jr.
Environmental Field Measurements Branch
NASA Langley Research Center
Hampton, VA 23665

J. P. Kahler
U.S. Air Force
Headquarters Air Weather Service
Scott Air Force Base, IL 62225

1. Introduction

The Taylor analysis for single particle dispersion can be used for large distances only if the values of spectral scales and standard deviations of fluctuating velocity components (σ_u, σ_v, and σ_w) are known. Hanna (1981A) summarized some of the investigations and results of atmospheric boundary layer research which quantify the variation of spectral scales and σ_u, σ_v, and σ_w with height and stability.

---

* On assignment from the NOAA, U.S. Department of Commerce.

Savannah River Laboratory (SRL) computed spectral scales and σ_u, σ_v, and σ_w from wind data taken in 1973 at the SRL-WJBF-TV tower in Beech Island, SC. These data have been compared with Hanna's summarized equations and are presented here. The wind data at SRL were collected at elevations between 18 and 305 m to study the properties of atmospheric turbulence within and above the atmospheric surface layer into the planetary boundary layer (PBL).

2. Tower and Meteorological Instruments

The SRL-WJBF tower is a 366-m tower instrumented at six levels to collect wind and temperature information. The instrumentation is mounted on heavy booms extending about 3 m outward from the tower (direction 225° from north). Figure 1 shows the levels and kinds of instrumentation used in 1973 to collect meteorological data. A few changes in the tower instrument configuration have been made since then.

The temperature sensors are ~100 ohm platinum resistance wire thermometers. Because these thermometers have time constants of several seconds, they are of no value in measuring turbulent heat flux.

The wind instruments are Climet cup and bivane systems. The distance constant of the cup anemometers is about 1 m. Electronic averaging circuits for the photo-chopper of the cup anemometers reduce the frequency response to about 0.1 Hz (-3 db reduction for sine wave input). The bivanes have a damping ratio of 0.55 and a delay distance of 0.9 m.

Prior to the 16-day study, all instruments used were carefully calibrated and additional instruments were attached at the 18.3 m level of the tower. A fast response thermistor and a Gill u-v-w anemometer were supplied by Battelle Northwest Laboratory to measure turbulent heat flux. The thermistor had a time constant of less than 0.12 sec depending on wind speed. This instrument configuration for heat flux measurement was compared to simultaneous measurements by a sonic anemometer-thermometer. Unpublished test results at Battelle Northwest Laboratory showed that the two methods agreed closely. Surface friction velocity measured with the cup and bivane system or the Gill u-v-w anemometer were within ±10% (Weber, et al., 1975). Comparison between the Gill u-v-w anemometer and a sonic anemometer for measuring stresses has been documented by Horst (1973). A correction recommended by Horst was applied to the wind measurements of the Gill anemometer to account for cosine response.

A Gill u-v-w anemometer should be aligned so that the wind blows into the "open" end of the three sensor array. Light and variable winds are thus a problem because gusts reach the sensors from unfavorable directions. Constant monitoring of wind direction was necessary during the experiment so that data collection could be interrupted when unfavorable wind direction did affect the sensors.

Wind and temperature measurements were recorded from the tower during a 16-day period from May 13 to May 29, 1973. Periods of rain, fog, or other disturbances to the instruments were subsequently omitted from the data. Data were collected on magnetic tape and then subjected to careful editing prior to final analysis.

The data were time averaged over 40-minute periods. Out of a total of 239 forty-minute blocks of data, only 119 were deemed acceptable for analysis after quality control checks. These checks for bad data were as follows:

- Data were removed if a particular block did not contain a full 40 minutes of data.
- Forty-minute blocks were removed if an upward transport of momentum was indicated (caused by low-level jets or other anomolous wind profiles).
- Blocks were rejected during laminar and nearly laminar flow cases (evidenced by vertical velocity fluctuation $\sigma_w < 0.01$ m/sec). These laminar flow cases were real but are beyond the scope of the present investigation.
- Blocks were rejected during sunrise and sunset periods when the surface layer was in transition.

Atmospheric turbulence spectra were calculated using a Fast Fourier Transform (FFT) technique of Singleton (1969). Wind speed and direction were converted to components in a natural coordinate system recommended by Kaimal and Touart (1967). In this system, the x axis was oriented along the mean wind vector, the y axis was oriented perpendicular to the x axis, and, in the horizontal plane, the z axis was oriented perpendicular to the x and y axes so as to form a right-hand coordinate system. It is important to note that in the natural coordinate system, the mean wind vector does not necessarily lie in the horizontal plane so that each 40-minute data block and anemometer level has its own unique coordinate system.

Time series composed of fluctuating velocity components were multiplied by a cosine taper data window over the beginning and final 10% of each 40-minute time series. This data window is used to reduce spectral leakage as suggested by Bingham, et al (1967). The FFT was applied to the tapered data and then raw power spectrum estimates were made. Autocorrelation values were then obtained by applying an inverse FFT. A Parzen lag window was applied to the autocorrelation values followed by another application of the FFT in order to obtain smoothed power spectral density estimates. Finally, a correction was made for the effect of the cosine taper data window (Bendat and Piersol, 1971). No linear or quadratic trends were removed from the individual time series.

3. Terrain

The WJBF tower is in the rural community of Beech Island, SC where there is a variety of land use in the immediate vicinity. Along any given azimuth, the gently rolling terrain is covered with pine tree forests (average height ~12 m), pastures, cultivated fields, and clearings of waist-high scrub. The Savannah River flows within 5.6 km to the west and within 9.7 km to the south of the tower. Long Branch, an intermittent stream, flows from northwest to southeast with its closest approach to the tower at about 610 m (Figure 2).

4. Properties of Velocity Spectra

Turbulence energy spectra give a rough representation of eddy size ranges active during dispersion. The energy spectrum is derived from the auto-correlation function by a Fourier cosine transform and the two functions form a Fourier transform pair:

$$F_E(n) = 4 \int_0^\infty R_E(\tau) \cos 2\pi n\tau \, d\tau, \tag{1}$$

$$R_E(\tau) = \int_0^\infty R_E(n) \cos 2\pi n\tau \, dn. \tag{2}$$

The integral scale of turbulence is defined as

$$T_E = \int_0^\infty R_E(\tau) d\tau. \tag{3}$$

The largest contribution to the integral is normally made by the larger eddies in the turbulent fluid.

When the power spectrum is plotted in the common meteorological representation [ln(n) versus n $F_E(n)$] the power for a given frequency interval is equal to the power in the corresponding frequency band from an n versus $F_E(n)$ plot. The maximum of the spectrum when plotted as ln(n) versus $nF_E(n)$ is reasonably easy to estimate. In recent years, the use of the spectral maximum frequency in diffusion computations has become more important because it can help specify the diffusivity through methods advocated by Pasquill (1974) and Hanna (1968, 1978A). For the vertical eddy diffusivity, the result is

$$K_z = \beta i_w \sigma_w \ell_{Ew} \tag{4}$$

where i_w is the intensity of turbulence for the vertical component i.e., $i_w = \sigma_w/\bar{u}$, σ_w is the standard deviation of the vertical velocity fluctuations, β is the ratio of the Lagrangian time scale T_L to the Eulerian time scale T_E, and ℓ_{Ew} is the Eulerian length scale for the vertical component, i.e., $\ell_{Ew} = T_{Ew}\bar{u}$. Earlier work summarized by Pasquill (1974) has shown that ℓ_{Ew} and λ_{mw} are related linearly.

For all spectra, the frequency n_m corresponding to the spectral maximum was obtained by computing a regression curve through 10 points of the spectrum and then interpolating to estimate the frequency at the maximum. That frequency was in turn converted to a wavelength λ_m. The Eulerian length scale (ℓ_E) was obtained by integrating the correlation function over the frequency range considered using the trapezoidal rule. Whenever the correlation function did not approach zero at large time lags, no value of ℓ_E was computed for the time period.

5. Summary of Hanna's 1981A Paper

Hanna's paper (1981A) succinctly summarized much of the present knowledge of PBL theory and measurement. Since his equations are used here to compare with the SRL measurements, a list of those equations is provided for convenient reference.

Taylor (1921):

$$\sigma_y^2 = 2\,\sigma_v^2\,T_{Lv}^2\left(t/T_{Lv} - 1 + \exp(-t/T_{Lv})\right) \qquad (5)$$

where σ_y is the standard deviation of the crosswind distribution of concentration, σ_v is the standard deviation of the crosswind component of velocity fluctuations in a natural coordinate system, and T_{Lv} is the Lagrangian time scale of the crosswind component of velocity.

Hanna (1978B):

$$v'(t + \Delta t) = v'(t)\ \exp\left(-\Delta t/T_{Lv}\right) + v'' \qquad (6)$$

where v' is the fluctuation of the lateral component of wind velocity.

Hay-Pasquill (1959) & Pasquill (1974)

$$T_{Lu,v,w}\ /T_{Eu,v,w} = \beta = 0.6/i_{u,v,w} = 0.6\ \bar{u}/\sigma_{u,v,w.} \qquad (7)$$

Pasquill (1974) and Hanna (1981A and 1981B)

$$T_{Eu,v,w} = 0.16\ \lambda_{mu,v,w}/\bar{u},$$
$$T_{Lu,v,w} = 0.96\ \lambda_{mu,v,w}/\sigma_{u,v,w.} \qquad (8a,b)$$

As noted above, the scales λ_m and ℓ_E can be related to one another. In order to restrict the plots to a reasonable number, it was decided to present results for only one of these two scales. It was felt that λ_m could be estimated more accurately than ℓ_E so only λ_m is presented in the plots, although the equations that follow are often written in terms of ℓ_E or T_E.

Unstable PBL

Deardorff (1970):

$$w_* = u_*\ \left(-z_i/0.4\ L\right)^{1/3} \qquad (9)$$

where w_* is the convective scaling velocity, u_* is the surface friction velocity, z_i is the depth of the mixed layer, and L is the Monin-Obukhov length scale.

Panofsky, et al (1977):

$$\sigma_u = \sigma_v = u_* \left(12 - 0.5\ z_i/L\right)^{1/3} \tag{10}$$

Irwin (1979) and Panofsky, et al (1977):

$$\sigma_w = 0.96\ w_* \left(3z/z_i - L/z_i\right)^{1/3},\ z/z_i < 0.03 \tag{11}$$

$$\sigma_w = w_* \min \left(0.96\ (3z/z_i - L/z_i)^{1/3},\right.$$
$$\left. 0.763\ (z/z_i)^{0.175}\right);\ 0.03 < z/z_i < 0.4 \tag{12}$$

$$\sigma_w = 0.722\ w_* \left(1 - z/z_i\right)^{0.207},\ 0.4 < z/z_i < 0.96, \tag{13}$$

$$\sigma_w = 0.37\ w_*,\ 0.96 < z/z_i < 1. \tag{14}$$

Kaimal, et al (1976):

$$T_{Lu} = T_{Lv} = 0.15/\left(\sigma_u/z_i\right) \tag{15}$$

$$T_{Lw} = 0.1\ \left(z/\sigma_w\right)/$$

$$0.55 + 0.38\left((z - z_o)/L\right) \quad \begin{matrix} z/z_i < 0.1 \\ \text{and} \\ -(z - z_o)/L < 1, \end{matrix} \tag{16}$$

$$T_{Lw} = \frac{0.59z}{\sigma_w} \quad \begin{matrix} z/z_i < 0.1 \\ \text{and} \\ -(z - z_o)/L > 1, \end{matrix} \tag{17}$$

$$T_{Lw} = \frac{0.15z_i\left(1 - \exp(-5z/z_i)\right)}{\sigma_w},\ z/z_i > 0.1. \tag{18}$$

Here z_o is the roughness length and all other parameters have been defined previously.

Stable PBL

Wyngaard (1975) and Rao and Snodgrass (1978):

$$h = a(u_*L/f)^{1/2}, \tag{19}$$

where h is the scale height of the stable boundary layer and f is the Coriolis parameter.

Minnesota PBL observations:

$$\sigma_w = \sigma_v = 1.3u_*(1 - z/h), \tag{20}$$

$$\sigma_u = 2u_*(1 - z/h). \tag{21}$$

Caughey, et al (1979) and Hanna (1981A):

$$\lambda_{mu} = 1.5(zh)^{0.5}, \tag{22}$$

$$\lambda_{mv} = 0.7(zh)^{0.5}, \tag{23}$$

$$\lambda_{mw} = 1.0z^{0.8}h^{0.2}, \tag{24}$$

$$T_{Lu} = 0.15(zh)^{0.5}/\sigma_u, \tag{25}$$

$$T_{Lv} = 0.07(zh)^{0.5}/\sigma_v, \tag{26}$$

$$T_{Lw} = 0.10(z^{0.8}h^{0.2})/\sigma_w. \tag{27}$$

Neutral PBL

Wyngaard, et al (1974):

$$\sigma_u = 2.0u_* \left(\exp(-\tfrac{3}{2}fz/u_*)\right), \tag{28}$$

$$\sigma_v = \sigma_w = 1.3u_* \left(\exp(-fz/u_*)\right). \tag{29}$$

Hanna (1968):

$$T_L = \left(0.5/(\sigma_w/z)\right)/(1 + 15fz/u_*). \tag{30}$$

6. Discussion

In Section 7, 8, and 9 of this paper, the predictions of Equations 9-30 are tested against the parameters derived from the May 1973 measurements at the WJBF-SRL tower. Correlations of the measurements and predictions were computed to quantify the results of scatter diagrams shown in Figures 3-21. The correlation coefficient r is defined as

$$r = \frac{\sum_{i=1}^{n} X_i Y_i}{\left[\sum_{i=1}^{n} X_i^2 \sum_{i=1}^{n} Y_i^2\right]^{1/2}} \qquad (31)$$

where X_i is the deviation from the mean independent variable and Y_i is the deviation from the mean dependent variable. Equation (31) can also be used to define a nonparametric correlation coefficient. For the nonparametric correlation coefficient, one simply replaces the magnitude of X_i and Y_i by the corresponding ranks of the independent and dependent variables, respectively. This correlation coefficient between ranks is often called Spearman's ρ or, in this paper, ρ. The measured quantities were taken to be independent variables and the predicted variables to be dependent variables. Correlation coefficients can be interpreted as good (r or $\rho > 0.7$), intermediate ($0.4 < r$ or $\rho < 0.7$), or poor (r or $\rho < 0.4$). The results are discussed according to stability class in the sections that follow.

The statistical evaluations of Equations 9-30 were made using the forms as given without normalizing. Normalization is often done with similarity theory validation but the practice can lead to artificial correlation as reported by Pearson (1897) and Hicks (1978).

Parameter values on the right hand of Equations 9-30 are measured at the 18.3 meter level which was assumed to be representative of the true surface values.

7. The Unstable PBL

In order to test the relationships in Equations 10-18, it was necessary to estimate z_i because no direct measurement was available. Using radiosonde temperature soundings from Athens, GA, and cloud cover from Augusta, GA, a model by Garrett (1981) was used to compute z_i. The z_i value was in turn used in Equation 9 to estimate w_*. By comparing the model results for z_i to the Athens, GA, temperature soundings, some subjective feelings about the representativeness of the z_i values were gained. For this data set, the classical convective boundary layer did not exist in most cases. The mixed layer was well defined during only three of the sixteen days. However, statistical results for those three days were not significantly different than for the larger complete data set. Therefore, results for the complete unstable data set (as judged by $z/L < -0.05$) are presented here.

Figures 3, 4, and 5 show plots of the right-hand sides of Equations 10-14 against measured σ_u, σ_v, and σ_w at each tower level. Figure 3 for the longitudinal component σ_u and Figure 4 for the lateral component σ_v show intermediate agreement between theory and measurement, r is 0.61 and 0.63 for σ_u and σ_v, respectively. The results for σ_w in Figure 5 yield an r value of 0.57.

Equations 15-18 give predictions for Lagrangian time scales of the three velocity components. These equations were transformed via Equations 7 and 8b so as to be in terms of our measured λ_m values. The plots in Figures 6 and 7 show that the results are poor for λ_{mu} and λ_{mv}. Correlation coefficients are -0.11 and 0.01 for those two length scales. The correlation coefficient between λ_{mw} calculated and the same quantity measured is 0.59, indicating better correlation. The plotted results for λ_{mw} are shown in Figure 8. In most cases, the measured λ_{mw} is less than the calculated value. We do not have an explanation for this occurrence this time.

8. The Stable PBL

In order to test the measurements against similarity theory predictions for the stable planetary boundary layer, it was necessary to estimate the height of the stable layer h from the parameters u_* and L. Since one of the temperature profile sensors

near the surface was faulty, it was necessary to use other methods for estimating h. Two formulae were available for estimating h, one by Venkatram (1980),

$$h = B\ u_*^{3/2} \qquad (32)$$

and the other from Equation 19.

Using u_* measurements from the Gill anemometer on the tower, the plot in Figure 9 was made of h from Equation 32 vs. h from Equation 19. Equation 32 predicts higher values of h than does Equation 19 by a factor of 2.25, but the correlation coefficient between height estimates is reasonably high (0.73).

For consistency, Equation 19 was used with Equations 20 and 21 to predict σ_w, σ_v, and σ_w. Figures 10, 11, and 12 show σ_u vs. Equation (21) and σ_v and σ_w vs. Equation (20). All measured parameters are from cup anemometer and bivane measurements at six levels. The results give correlations of 0.40, 0.45, and 0.49 for σ_u, σ_v, and σ_w, respectively.

Figures 13, 14, and 15 show the nondimensional spectral scales λ_{mu}, λ_{mv}, and λ_{mw} derived from the measurements of cup anemometers and bivanes at six levels plotted against Equations 22, 23, and 24. Measurements and calculations have an r value rated as intermediate except for the longitudinal component. The values of r for λ_{mu}, λ_{mv}, and λ_{mw} are 0.83, 0.61, and 0.54, respectively.

Figures 13 and 14 show λ_{mu} and λ_{mv} measured values which are mostly greater than those same values computed by Caughey's (1979) formulae. Caughey's (1979) formulae are based on velocity records from which the trend was removed so that they represent micrometeorological energy. This is a plausible explanation for the greater value of the measured quantities, since trends were not subtracted from the SRL-WJBF data.

9. The Neutral PBL

In describing the neutral planetary boundary layer, Hanna (1981A) mentioned the dearth of data, particularly for the upper part of the PBL. It was anticipated that the SRL measurements would be of value in filling this void because a considerable number of observations were for near neutral conditions, based on $|z/L| < 0.05$. SRL measurements were compared to those of Wyngaard, et al (1974) given in Equations 28 and 29. The results of plotting predicted σ_u, σ_v, and σ_w in Equations 28 and 29 vs. the same quantities measured with cup anemometers and bivanes are shown in Figures 16, 17, and 18. The results gave reasonably good correlation coefficients of 0.73, 0.72, 0.70 for σ_u, σ_v, and σ_w, respectively.

Hanna's (1968) observations and theory on spectral scale for neutral conditions are repeated in this paper as Equation 30, and were tested with the SRL data. Six levels of measured λ_{mu}, λ_{mv}, and λ_{mw} are plotted against the predictions of Equation 30 and

shown in Figures 19, 20, and 21. (The right side of Equation 30 was multiplied by $\sigma_{u,v,w}/0.96$.) The plots for λ_{mu}, λ_{mv} and λ_{mw} show correlations of 0.68, 0.55, and 0.71, respectively.

10. CONCLUSIONS

Table 1 shows the summarized results for the correlation coefficients r and ρ for the three stability classes.

TABLE 1

	σ_u	σ_v	σ_w	λ_{mu}	λ_{mv}	λ_{mw}
r Unstable	0.61	0.63	0.57	-0.11	0.01	0.59
ρ Unstable	0.66	0.66	0.57	-0.07	0.01	0.53
r Stable	0.40	0.45	0.49	0.83	0.61	0.54
ρ Stable	0.44	0.44	0.48	0.83	0.61	0.52
r Neutral	0.73	0.72	0.70	0.68	0.55	0.71
ρ Neutral	0.72	0.71	0.72	0.72	0.62	0.75

There was fair agreement between measurements and various theories except for the unstable class. The correlation coefficient range was between 0.40 and 0.83 for all parameters except λ_{mu}, and λ_{mv}, in unstable conditions. The reasons for poor correlation between measured and predicted values of λ_m in unstable conditions might have been that well defined mixed layers were not present during the periods when data were recorded. It is also possible that trends in the unstable cases masked the true peaks of the spectra.

The experimental measurements for this study were taken over terrain with farms and crops, broken by pine forests and streams. This terrain is typical of parts of South Carolina and Georgia and other southeastern states. Because of terrain complexity, one should not expect excellent agreement between measurements and theory.

The experiments in this study have given some quantification of the agreement one could expect between measurements in nonhomogenous and theory designed for long uniform fetches.

11. ACKNOWLEDGMENTS

The information contained in this article was developed during the course of work under Contract No. DE-AC09-76SR00001 with the U.S. Department of Energy.

The field program in May 1973 and some of the subsequent data analysis was supported by EPA under Grant No. 804278.

J. F. Schubert was particularly helpful during the period when data were being collected in 1973. A. J. Garrett and M. M. Pendergast of the Savannah River Laboratory made helpful suggestions during the analysis of these data. J. H. Weber pointed out the Pearson (1897) reference and made several suggestions in the interpretation of the statistical results.

Jason Ching of EPA's Meteorology and Assessment Division was particularly helpful during the writing of this paper.

Thanks to J. E. Beach of Savannah River Laboratory's Technical Information Service for his help in the preparation of this paper.

SYMBOLS

$F_E(n)$	the normalized one-dimensional spectral density function at a fixed point in space.
ℓ_E	the Eulerian integral length scale of turbulence.
$\ell_{Eu,\ v,\ w}$	$\ell_{Ew} = \bar{u} \int_0^\infty R_{Ew}(\tau)\ d\tau$, etc.
n	frequency
n_m	the frequency at which the nS(n) vs ln(n) spectrum reaches its maximum value
$R_E(\tau)$	the Eulerian correlation function
$R_{Eu,\ v,\ w}$	$R_{Ew} = \int_0^\infty F_{Ew}(n) \cos 2\pi n\tau\ d\tau$, etc.
τ	time lag
T_E	Eulerian time scale
T_L	Lagrangian time scale
$x,\ y,\ z$	Cartesian coordinates in a natural coordinate system
$u,\ v,\ w$	velocity components in a natural coordinate system
$\sigma_u,\ \sigma_v,\ \sigma_w$	standard deviations of the velocity components in a natural coordinate system
λ	wavelength; $\lambda_m = \bar{u}/n_m$ (subscripts u, v, and w refer to longitudinal, lateral, and vertical components of the velocity spectrum
$\bar{u}$	magnitude of the mean vector wind at a given level
r	Pearson's correlation coefficient
ρ	Spearman's correlation coefficient
i_w	intensity of turbulence
h	scale height of the stable boundary layer
f	Coriolis parameter

β	ratio of Lagrangian and Eulerian time scales
L	Monin-Obukhov length - $\frac{u_*^3}{H} \frac{\rho_a c_p T}{kg}$
z/L	height of measurement divided by L
u_*	surface friction velocity $(\overline{-u'w'})^{1/2}$
H	vertical turbulent heat flux
ρ_a	air density
c_p	specific heat of air at constant pressure
T, T'	temperature and temperature fluctuation
t	time
k	Von Karman's constant
g	acceleration of gravity
z_i	depth of the unstable mixed layer
Θ	potential temperature
B	a constant

REFERENCES

Bendat, J. S., and A. G. Piersol, 1971: Random Data Analysis and Measurement Procedures. Wiley-Interscience, New York, 407 pp.

Berman, B. 1965: Estimating the longitudinal wind spectrum near the ground. Quart. J. Roy. Meteor. Soc., 91, 302 pp.

Bingham, C., M.D. Godfrey, and J. W. Tukey, 1967: Modern techniques of power spectrum estimation. Trans. IEEE Audio and Electroacoustics, AU-15, 56-66.

Caughey, J. J., and C. J. Readings, 1974. Vertical component of turbulence in convective conditions. Advances in Geophysics 18a, Academic Press, NY, 125-130.

Caughey, S. J., J. C. Wyngaard and J. C. Kaimal, 1979: Turbulence in the evolving stable boundary layer. J. Atmos. Sci., 36, 1041-1052.

Deardorff, J. A., 1970: Convective velocity and temperature scales for the unstable planetary boundary layer and for Rayleigh convection. J. Atmos. Sci., 27, 1211-1213.

Garrett, A. J., 1981: Comparison of observed mixed-layer depths to model estimates using observed temperatures and winds, and MOS forecasts. J. Appl. Meteor., 20, 1277-1285.

Hanna, S. R., 1968: A method of estimating vertical eddy transport in the planetary boundary layer using characteristics of the vertical velocity spectrum. J. Atmos. Sci., 25, 1026-1033.

Hanna, S. R., 1978A: A review of the influence of new boundary layer results on diffusion prediction techniques. ATDL Contribution File No. 7815, Air Resources Atmospheric Turbulence and Diffusion Laboratory, Oak Ridge, TN, 119-126.

Hanna, S. R., 1978B: Some statistics of Lagrangian and Eulerian wind fluctuations. J. Appl. Meteor., 18, 518-525.

Hanna, S. R., 1980: Effect of release height on σ_y and σ_z, ATDL Report 80/24, Annual Report to NRC. ATDL, P.O. Box E, Oak Ridge, TN, 108 pp.

Hanna, S. R., 1981A: Turbulent energy and Lagrangian time scales in the planetary boundary layer. Extended Abstracts of the Fifth Symposium on Turbulence, Diffusion, and Air Pollution. March 9-13, 1981, Atlanta, GA. Published by the American Meteorological Society, Boston, MA., 276 pp.

Hanna, S. R., 1981B: Lagrangian and Eulerian time scale relations in the daytime boundary layer. J. Applied Meteor., 20, 242-247.

Hay, J. S. and F. Pasquill, 1959: Diffusion from a fixed source at a height of a few hundred feet in the atmosphere, J. Fluid Mech, 2, 299 pp.

Hicks, B. B., 1978: Some limitations of dimensional analysis and power laws. Bound. Lay. Meteor., 14, 567-569.

Horst, T. W., 1973: Corrections for response errors in a three component propeller anemometer. BNWL-SA-4262, Battelle Memorial Institute, Pacific-Northwest Laboratories, Richland, WA, 30 pp.

Irwin, J. S., 1979: Estimating plume dispersion - a recommended generalized scheme. Preprints of the Fifth Symposium on Turbulence, Diffusion, and Air Pollution. January 15-18, 1979, Reno, Nevada. Published by the American Meteorological Society, Boston, MA, 677 pp.

Kaimal, J. C., and C. N. Touart, 1967: Critical examination of transformation to vector-mean coordinates. J. Appl. Meteor., 6, 583-587.

Kaimal, J. C., J. C. Wyngaard, D. A. Haugen, O. R. Cote, and Y. Y. Izumi, 1976: Turbulence structure in the convective boundary layer. J. Atmos. Sci, 33, 2152-2169.

Nieuwstadt, F. T. M., 1980. A rate equation for the inversion height in a nocturnal boundary layer. J. Appl. Meteor. 19. 1445-1447.

Nieuwstadt, F. T. M., 1981. The height of the stable boundary layer: theory and observations. Fifth symposium on turbulence, diffusion, and air pollution, Amer. Meteor. Soc. Boston, MA, 104-105.

Panofsky, H. A., H. Tennekes, D. H. Lenschow, and J. C. Wyngaard, 1977: The characteristics of turbulent velocity components in the surface layer under convective conditions. Bound. Lay. Meteor., 11, 355-361.

Pasquill, F., 1974: Atmospheric Diffusion, 2nd edition, Halsted Press, John Wiley and Sons, NY, 429 pp.

Pearson, K., 1897: Mathematical contribution to the theory of evolution on a form of spurious correlation which may arise when indices are used in the measures of organs. Proceedings of the Royal Society of London, Vol. LX, 489-502.

Rao, K. S. and H. F. Snodgrass, 1978: The structure of the nocturnal planetary boundary layer. ATDL Rept. 78/9, ATDL, P. O. Box E, Oak Ridge, TN., 17 pp.

Singleton, R. C., 1969: An algorithm for computing the mixed radix fast Fourier transform. Trans. IEEE Audio Electroaccoustics, AU-17 (2), 93-103.

Taylor, G. I., 1921: Diffusion by continuous movements. Proc. London Math. Soc. Ser. 2., 20, 196-212.

Taylor, R. J., J. Warner, and N. E. Bacon, 1970: Scale length in atmospheric turbulence as measured from an aircraft. Quart. J. Roy. Meteor. Soc., 96, 750-755.

Venkatram, A., 1980: Estimating the Monin-Obukhov length in the stable boundary layer for dispersion calculations. Bound. Lay. Meteor., 19. 481-485.

Weber, A. H., J. S. Irwin, J. P. Kahler, and W. B. Petersen, 1975: Atmospheric turbulence properties in the lowest 300 meters. Report No. EPA-600/4-75-004, Environmental Protection Agency, Research Triangle Park, NC, 153 pp.

Wyngaard, J. C., O. R. Cote and K. S. Rao, 1974: Modeling the atmopsheric boundary layer. Adv. in Geophys., 18A. Academic Press, NY, 193-211.

Wyngaard, J. C., 1975: Modeling the planetary boundary layer-extension to the stable case. Bound. Lay. Meteor., 9, 441-460.

Yamada, T, and S. Berman, 1979: A critical evaluation of a simple mixed-layer model with penetrative convection. J. Appl. Meteor., 18, 781-786.

Yu, T. W., 1978. Determining height of the nocturnal boundary layer. J. Appl. Meteor., 17, 28-33.

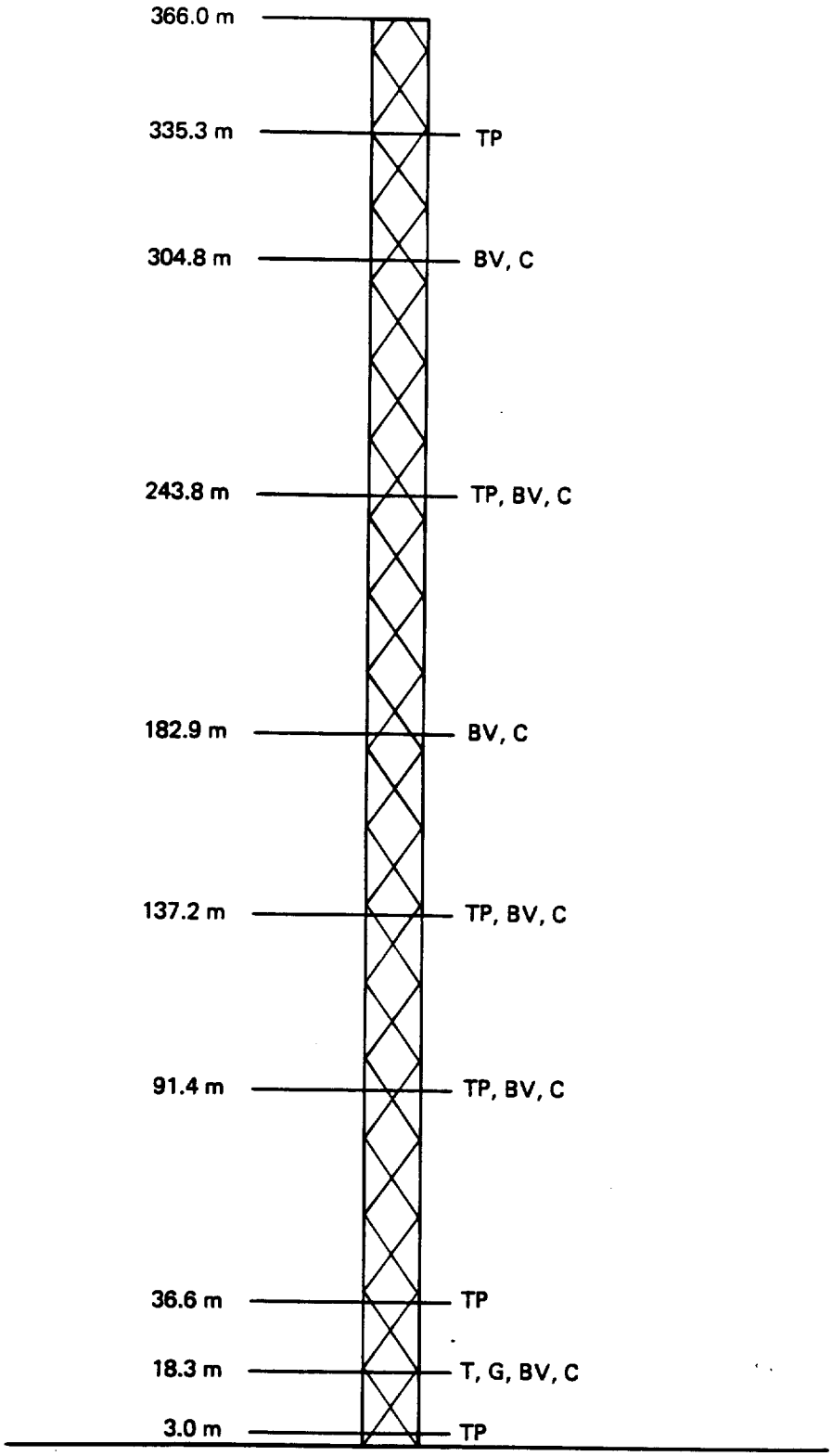

FIGURE 1. The SRL WJBF-TV Tower instrument configurations in 1973. The boom extension from the tower face was 3 m. TP - platinum resistance wire thermometer, T - thermistor, BV - Bivane, C - cup anemometer, G - Gill propeller anemometer.

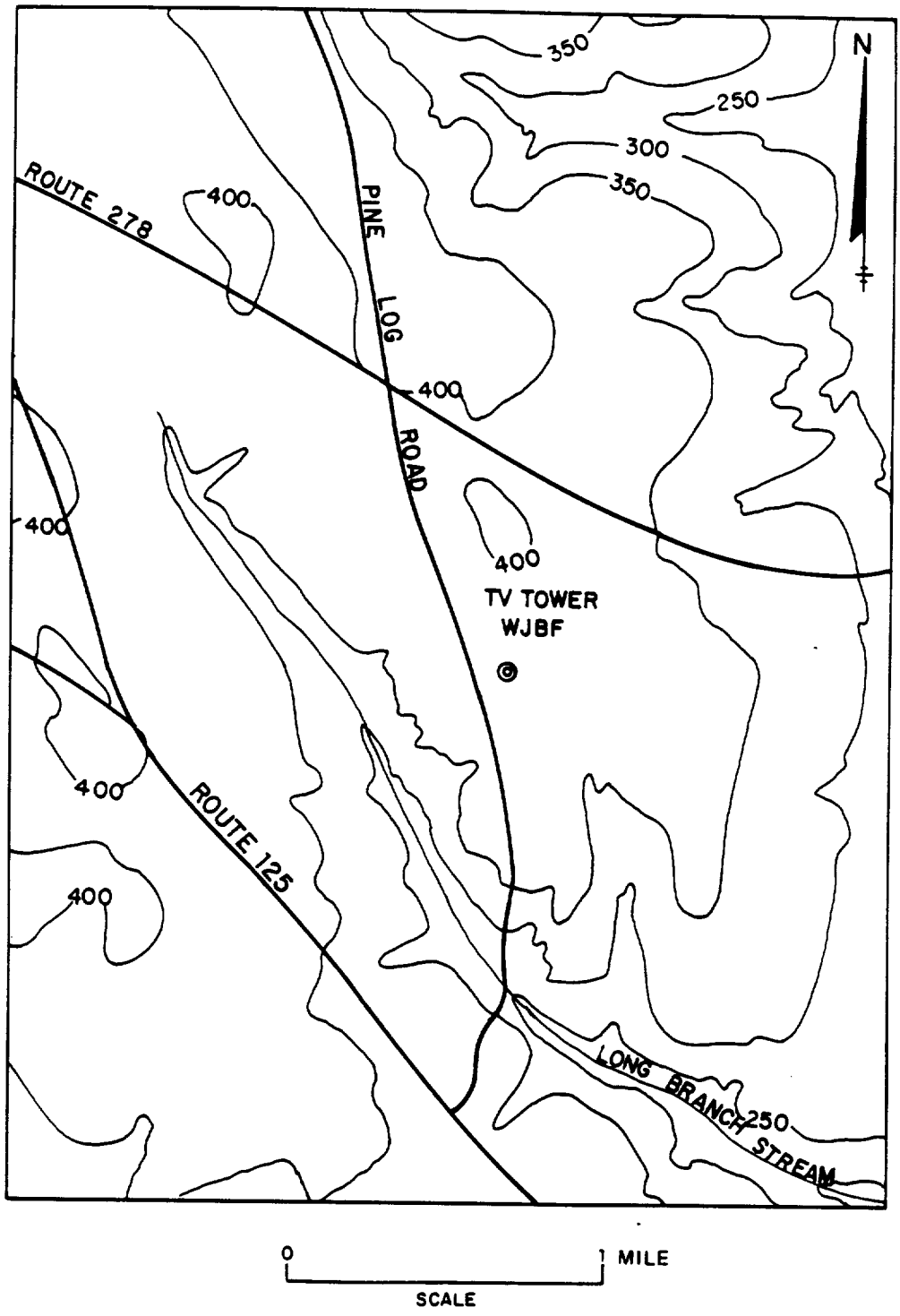

FIGURE 2. The Terrain at SRL WJBF tower. Contours are for every 50 feet.

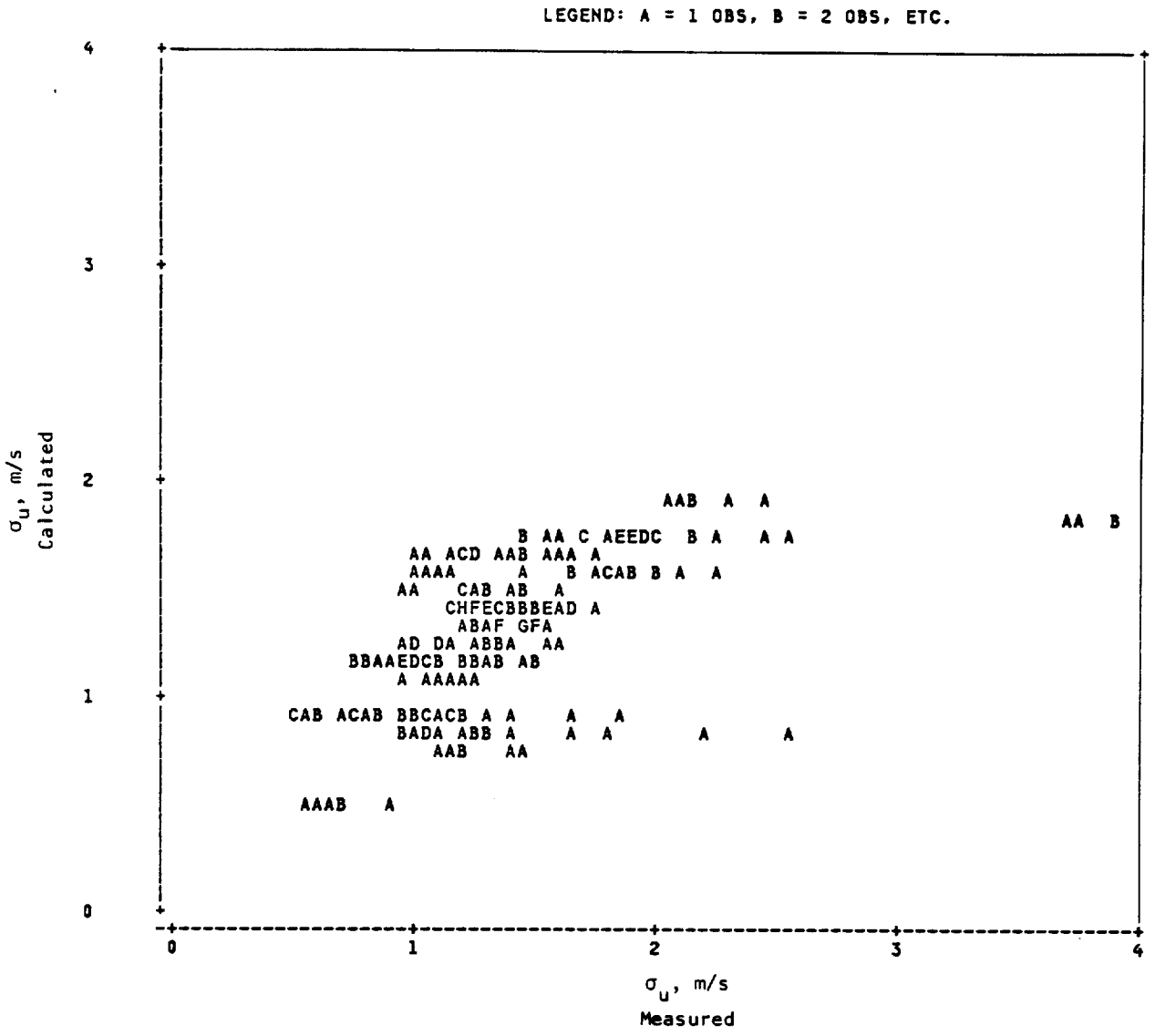

FIGURE 3. σ_u computed from Equation 10 using Gill propeller, thermistor, and resistance thermometer measurements vs. σ_u from measurements at six tower levels using cups and bivanes.

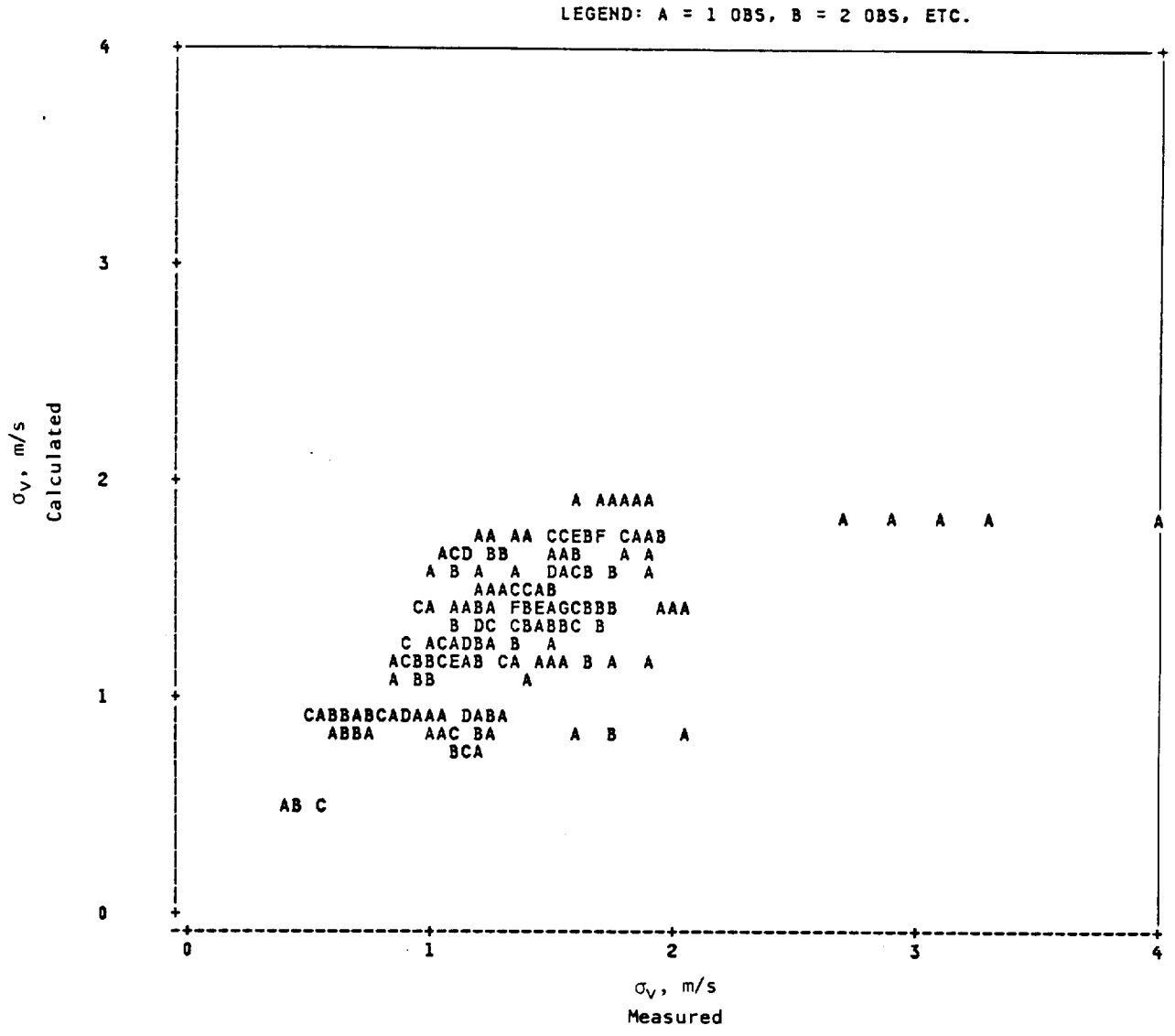

FIGURE 4. σ_v computed from Equation 10 using Gill propeller, thermistor, and resistance thermometer measurements vs. σ_v from measurements at six tower levels using cups and bivanes.

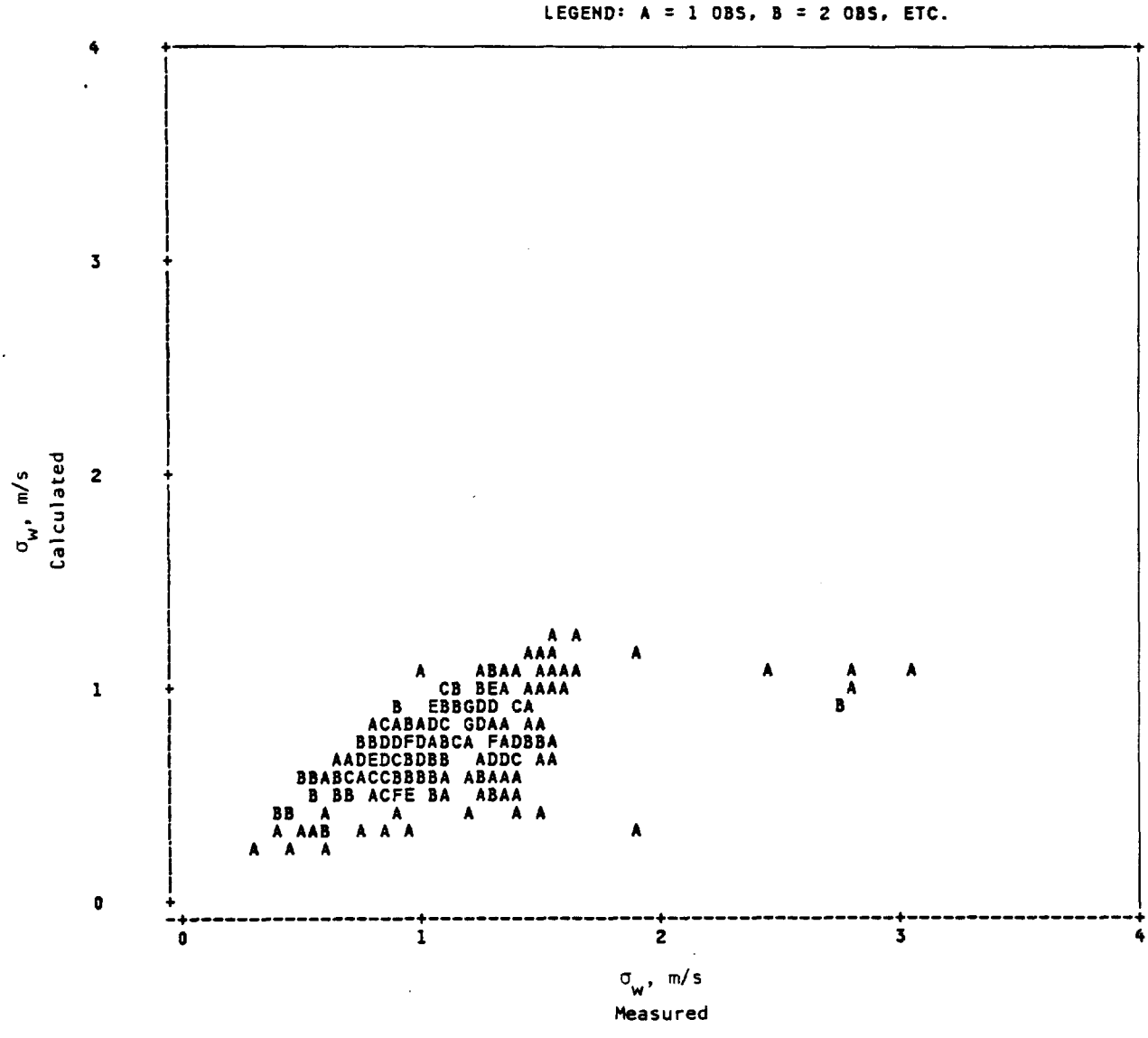

FIGURE 5. σ_w computed from Equations 11, 12, 13, and 14 using Gill propeller, thermistor, and resistance thermometer measurements vs. σ_w from measurements at six tower levels using cups and bivanes.

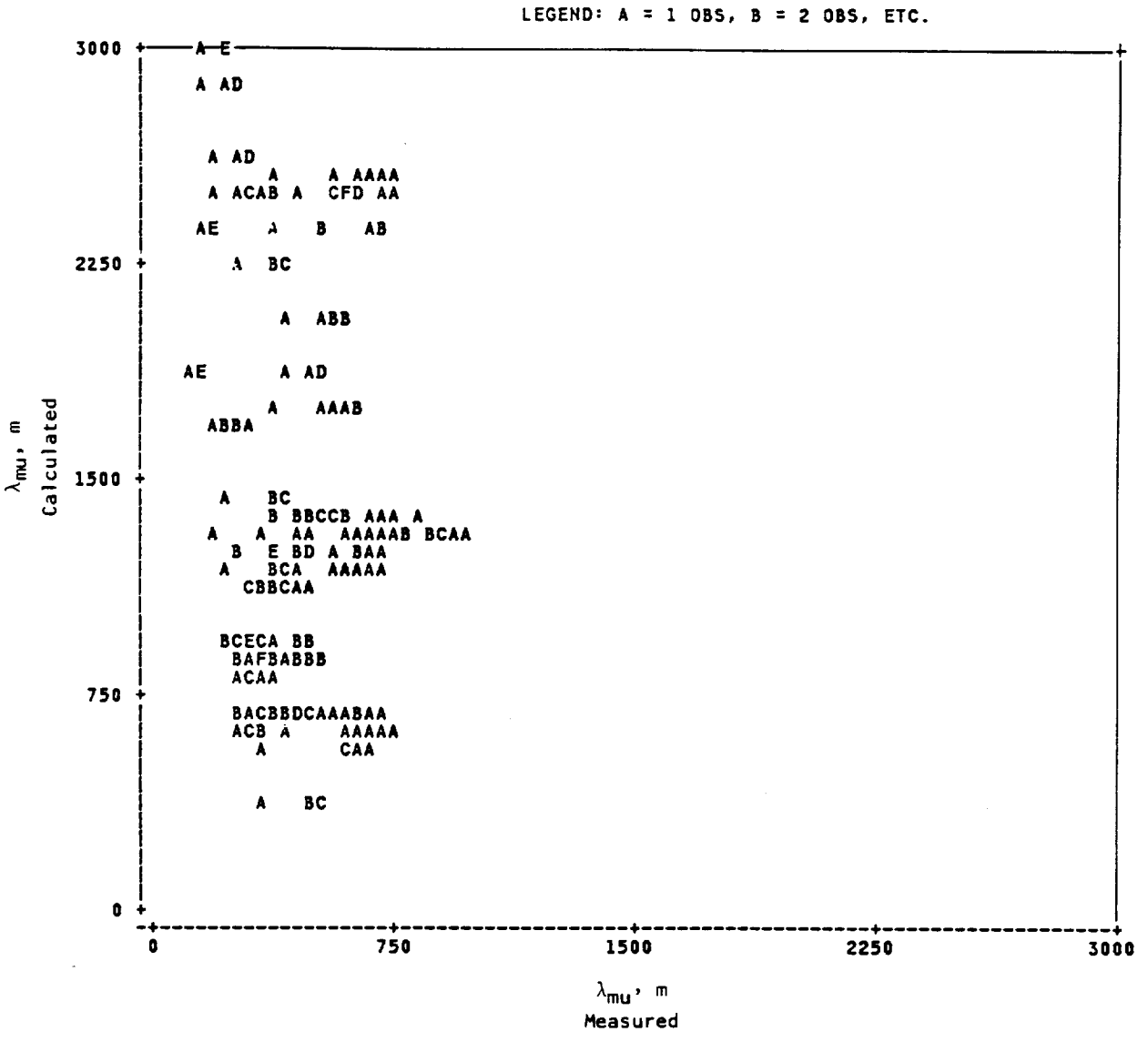

FIGURE 6. λ_{mu} computed from Kaimal, et al (1976) (Equations 8b and 15 of this paper) using Gill propeller and resistance thermometer measurements vs. λ_{mu} from measurements at six tower levels using cups and bivanes.

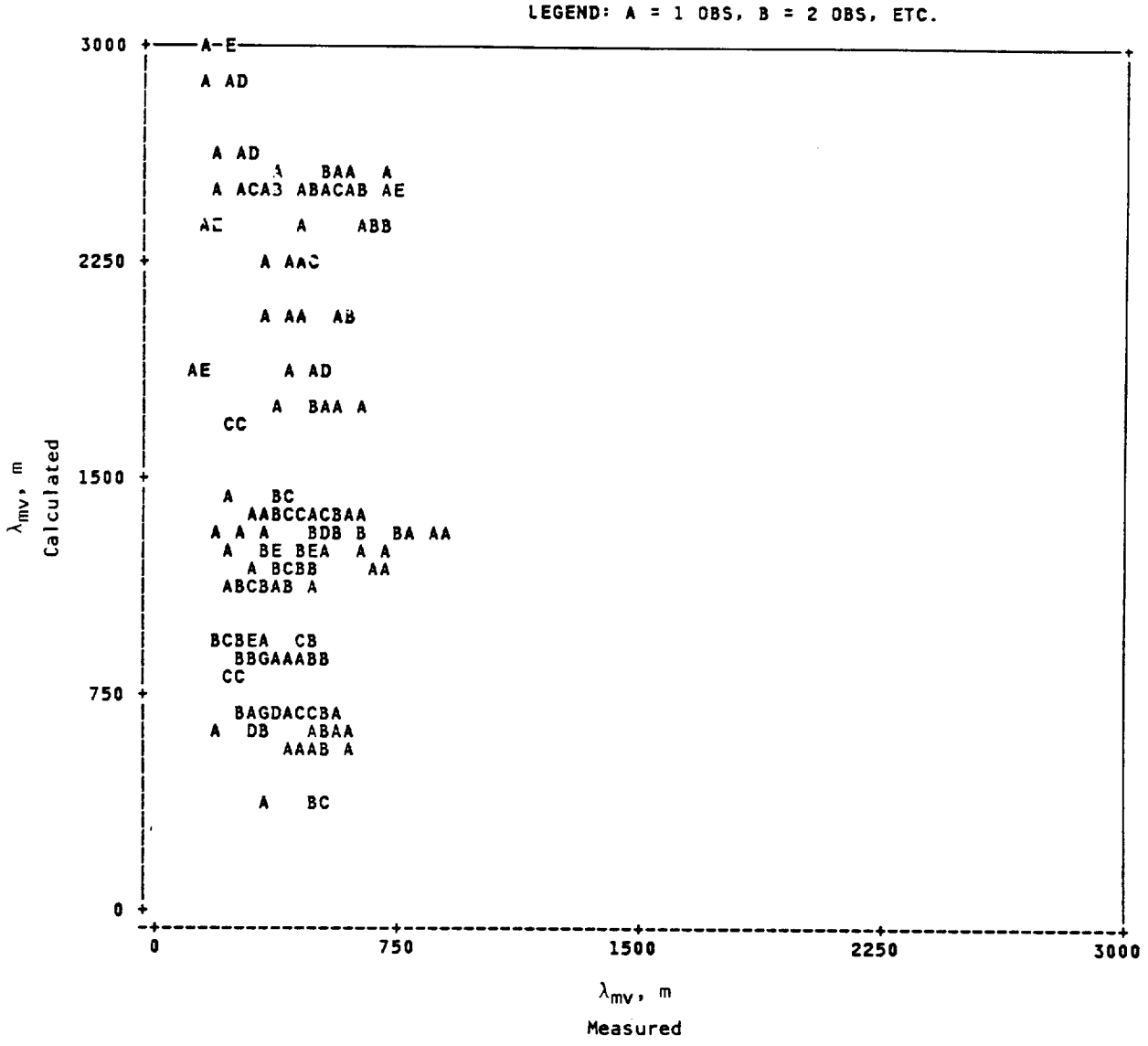

FIGURE 7. λ_{mv} computed from Kaimal, et al (1976) (Equations 8b and 15 of this paper) using Gill propeller and resistance thermometer measurements vs. λ_{mv} from measurements at six tower levels using cups and bivanes.

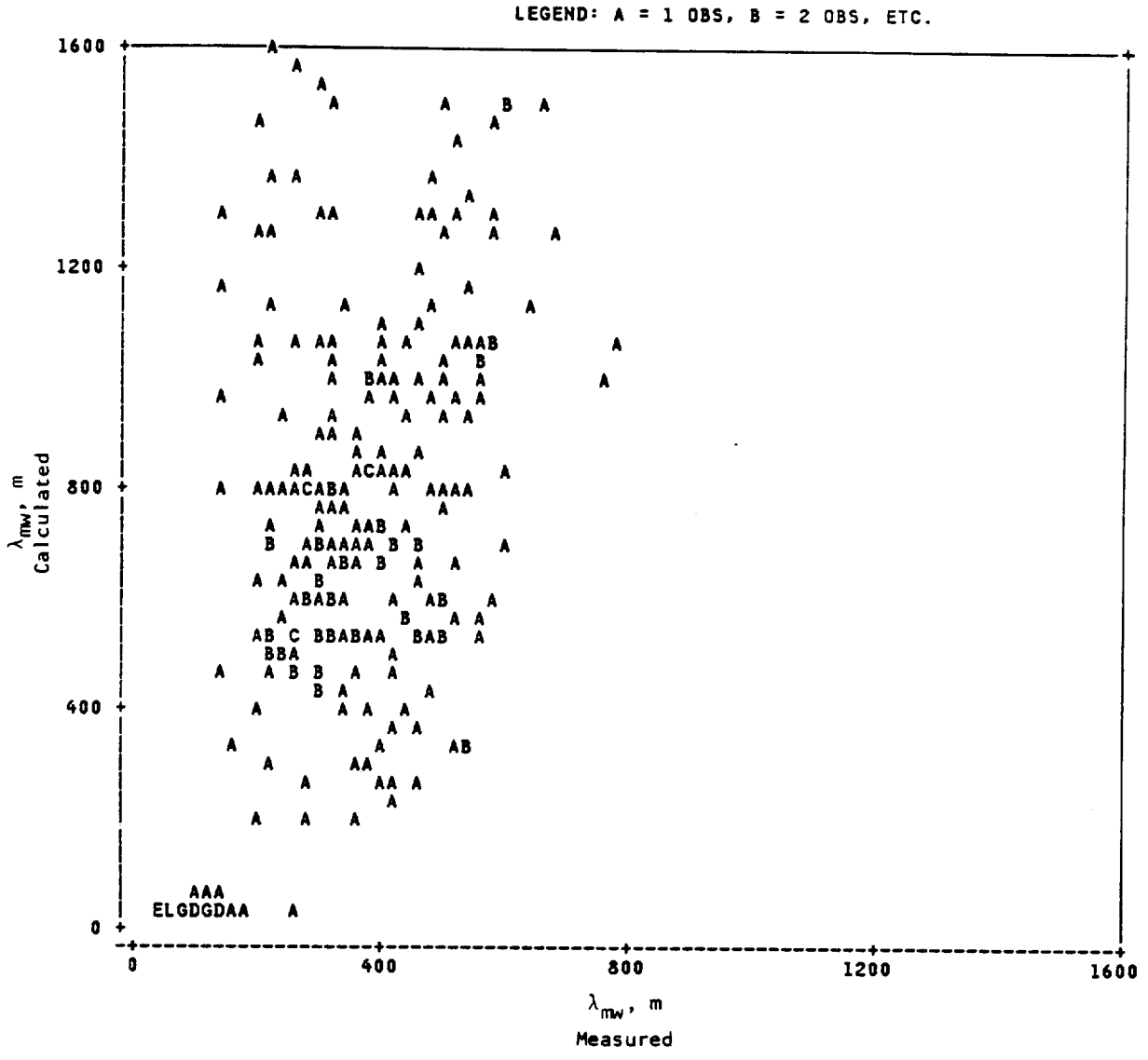

FIGURE 8. λ_{mw} computed from Kaimal, et al (1976) (Equation 8 of Kaimal) using Gill propeller and resistance thermometer measurements vs. λ_{mw} from measurements at six tower levels using cups and bivanes.

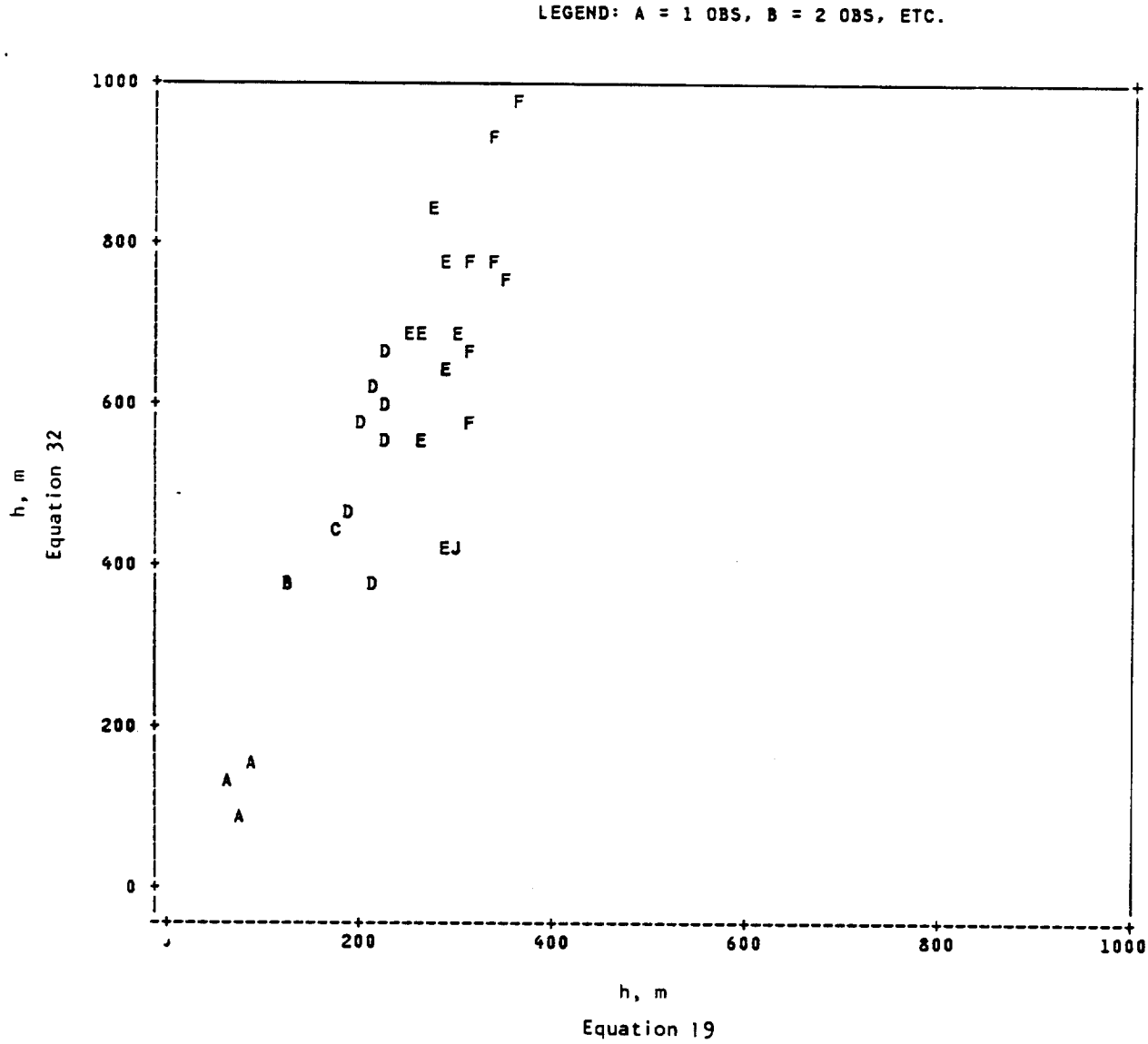

FIGURE 9. **h computed from Equation 32 vs. h computed from Equation 19 both using Gill propeller measurements.**

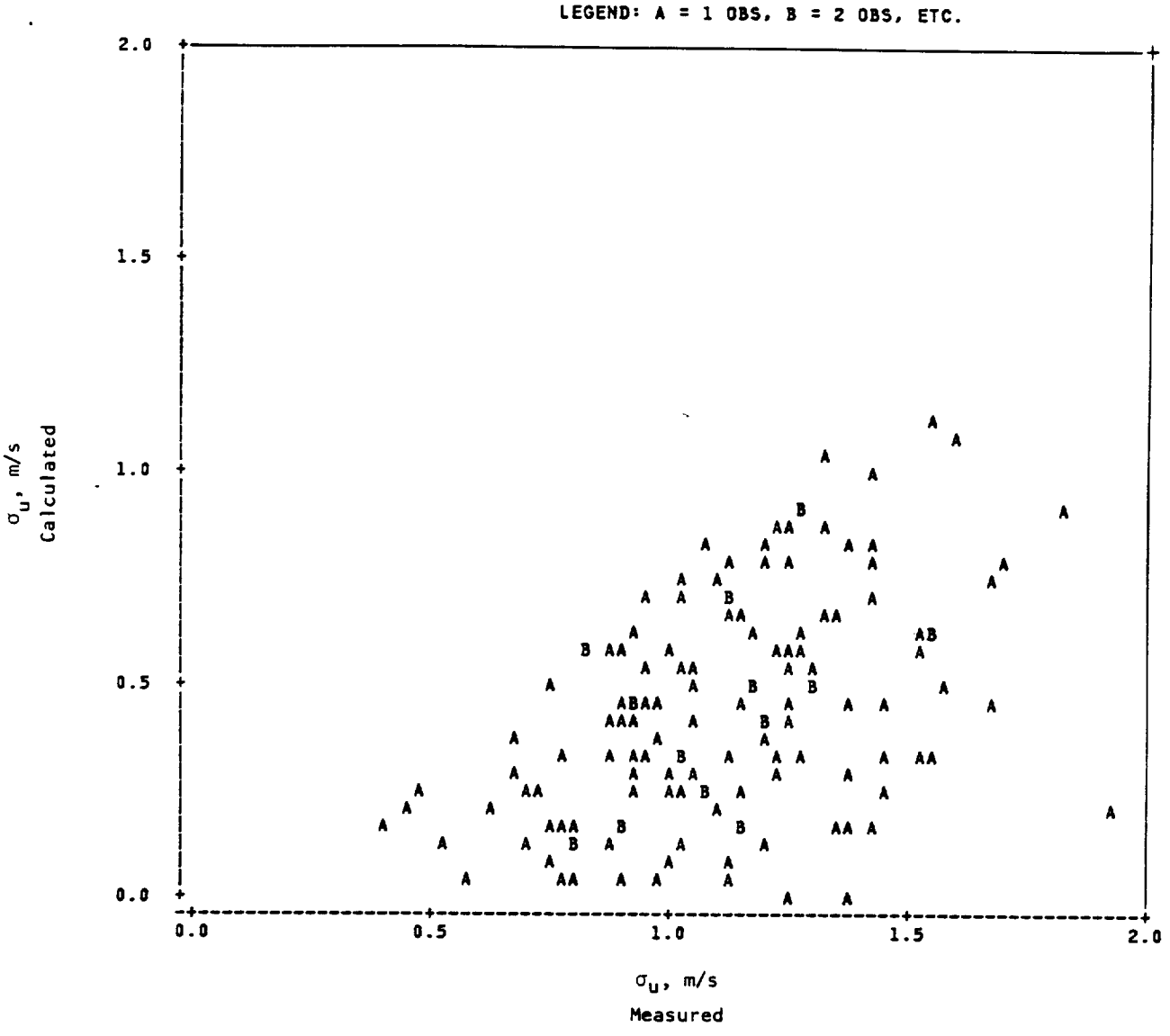

FIGURE 10. σ_u computed from Equations 21 and 19 using Gill propeller, thermistor, and resistance thermometer measurements vs. σ_u from measurements at six tower levels using cups and bivanes.

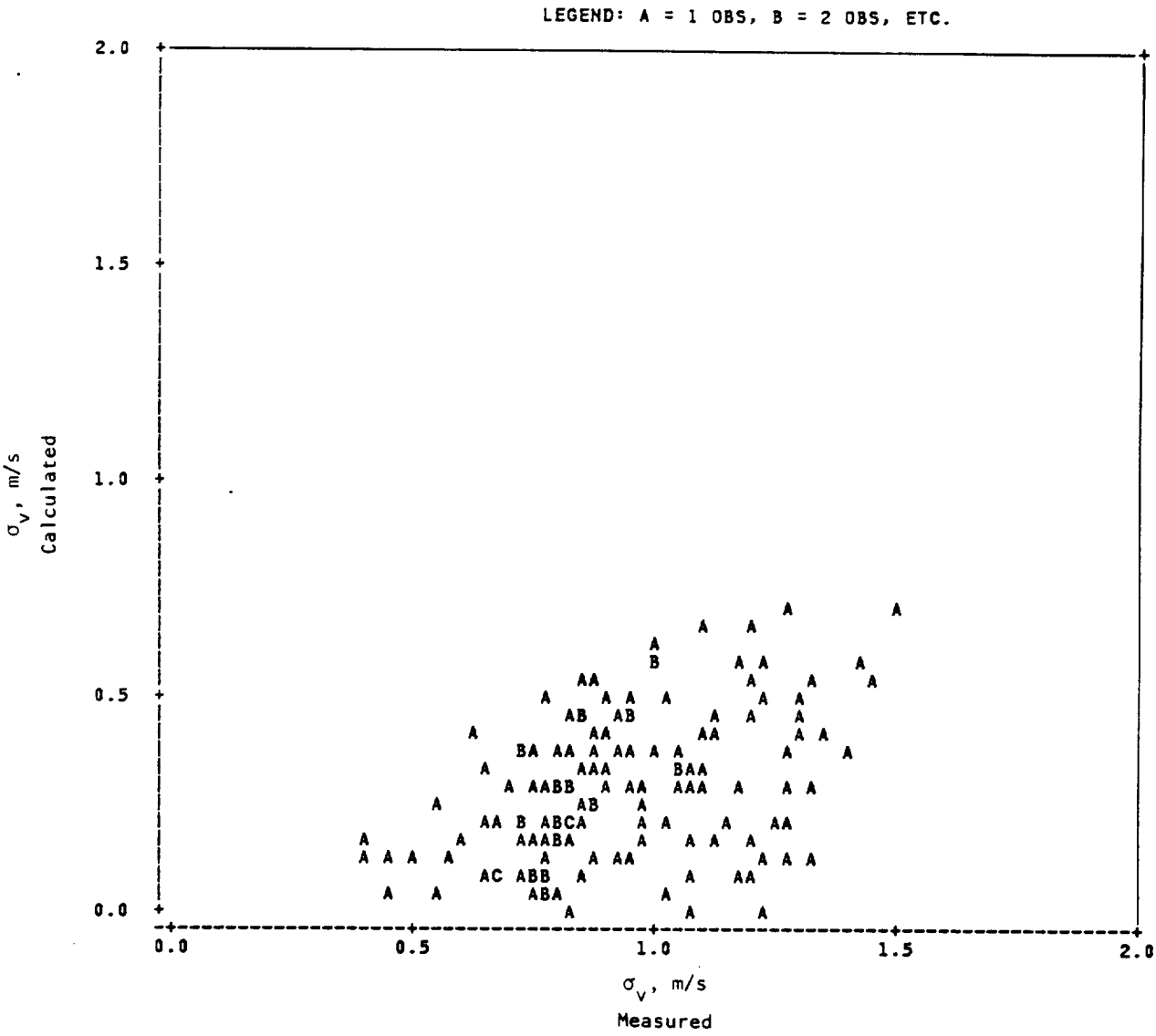

FIGURE 11. σ_v computed from Equations 20 and 19 using Gill propeller measurements vs. σ_v from measurements at six tower levels using cups and bivanes.

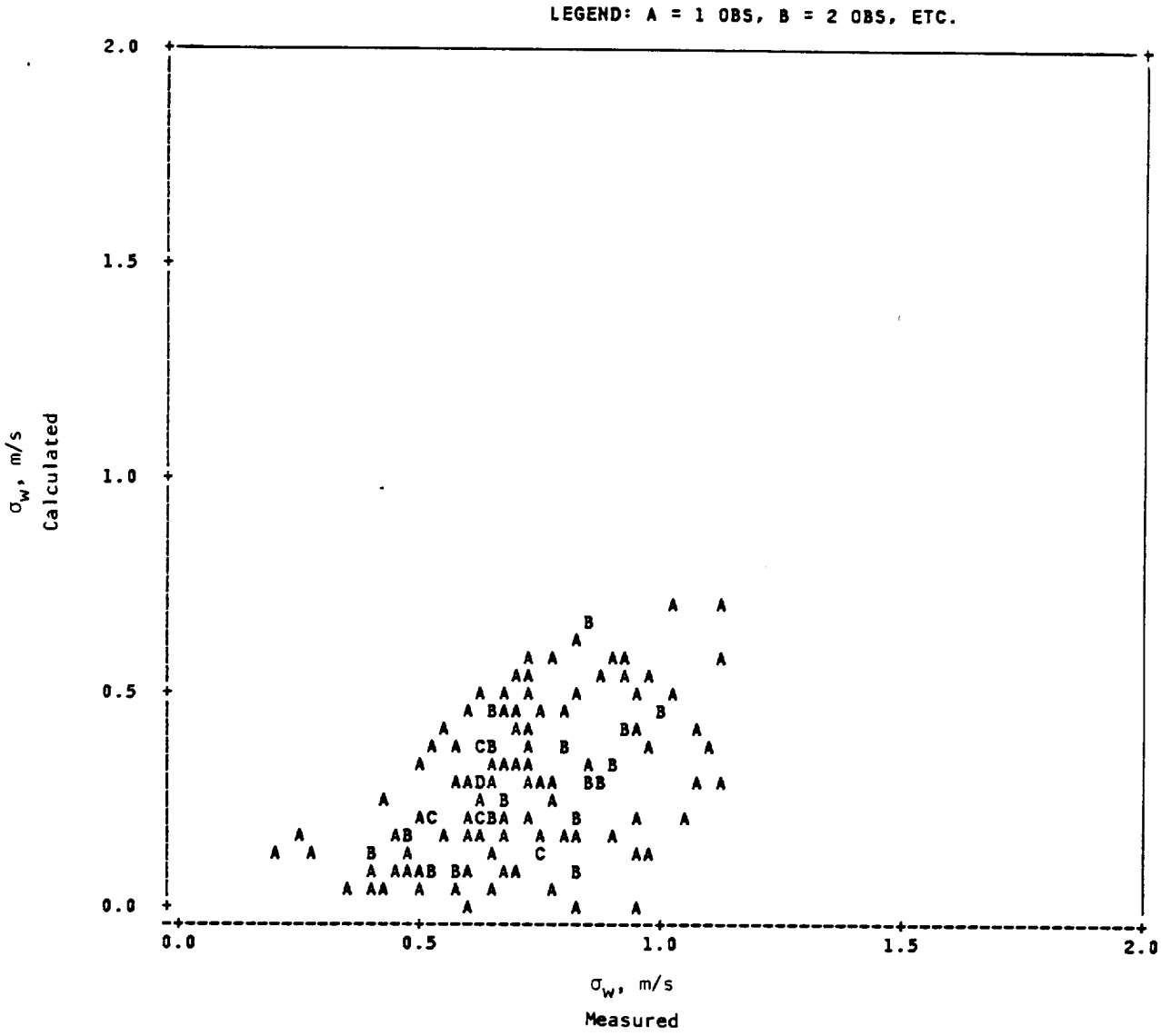

FIGURE 12. σ_w computed from Equations 20 and 19 using Gill propeller measurements vs. σ_w from measurements at six tower levels using cups and bivanes.

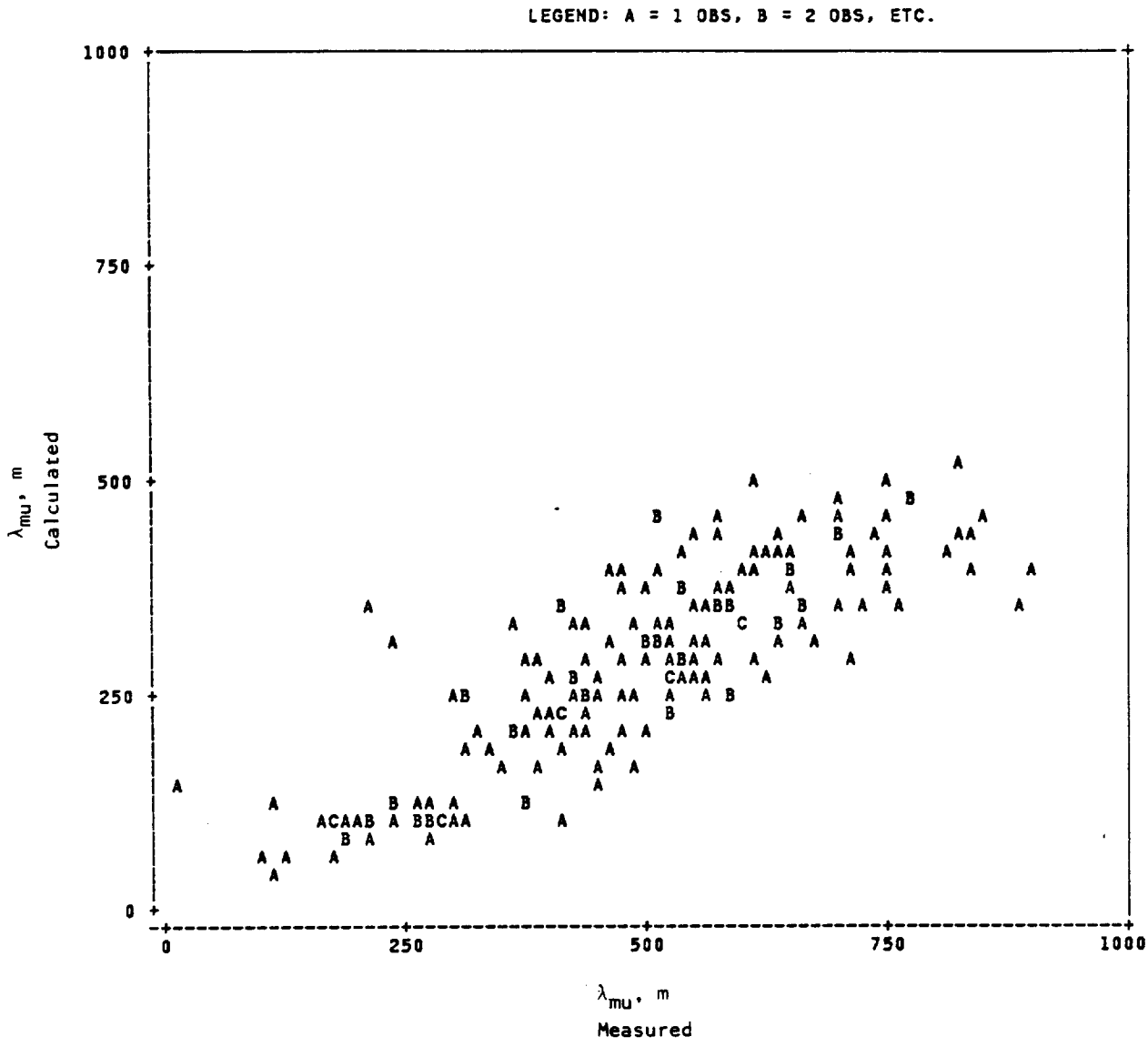

FIGURE 13. λ_{mu} computed from Equations 22 and 19 using Gill propeller measurements vs. λ_{mu} from measurements at six tower levels using cups and bivanes.

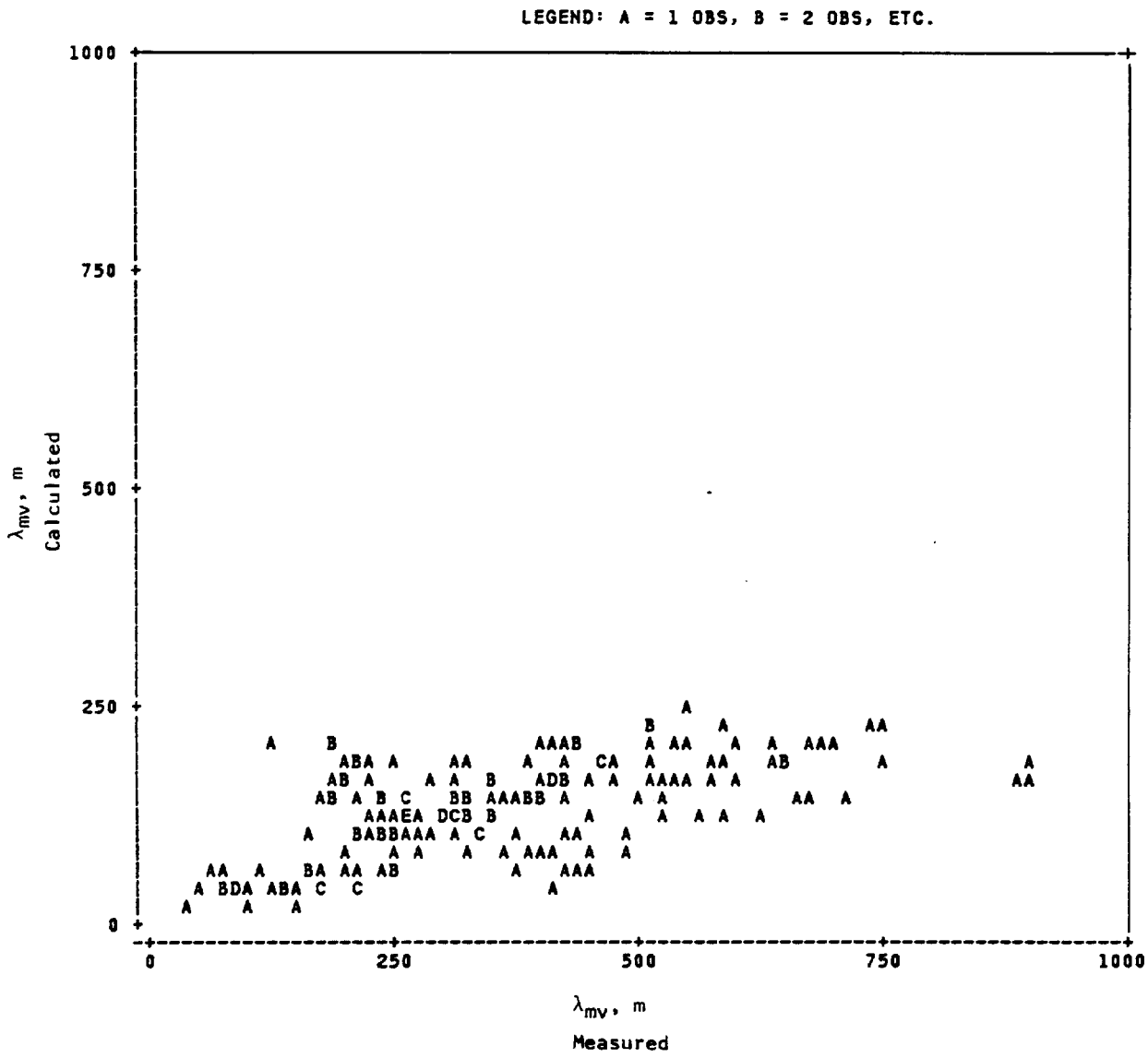

FIGURE 14. λ_{mv} computed from Equations 23 and 19 using Gill propeller measurements vs. λ_{mv} from measurements at six tower levels using cups and bivanes.

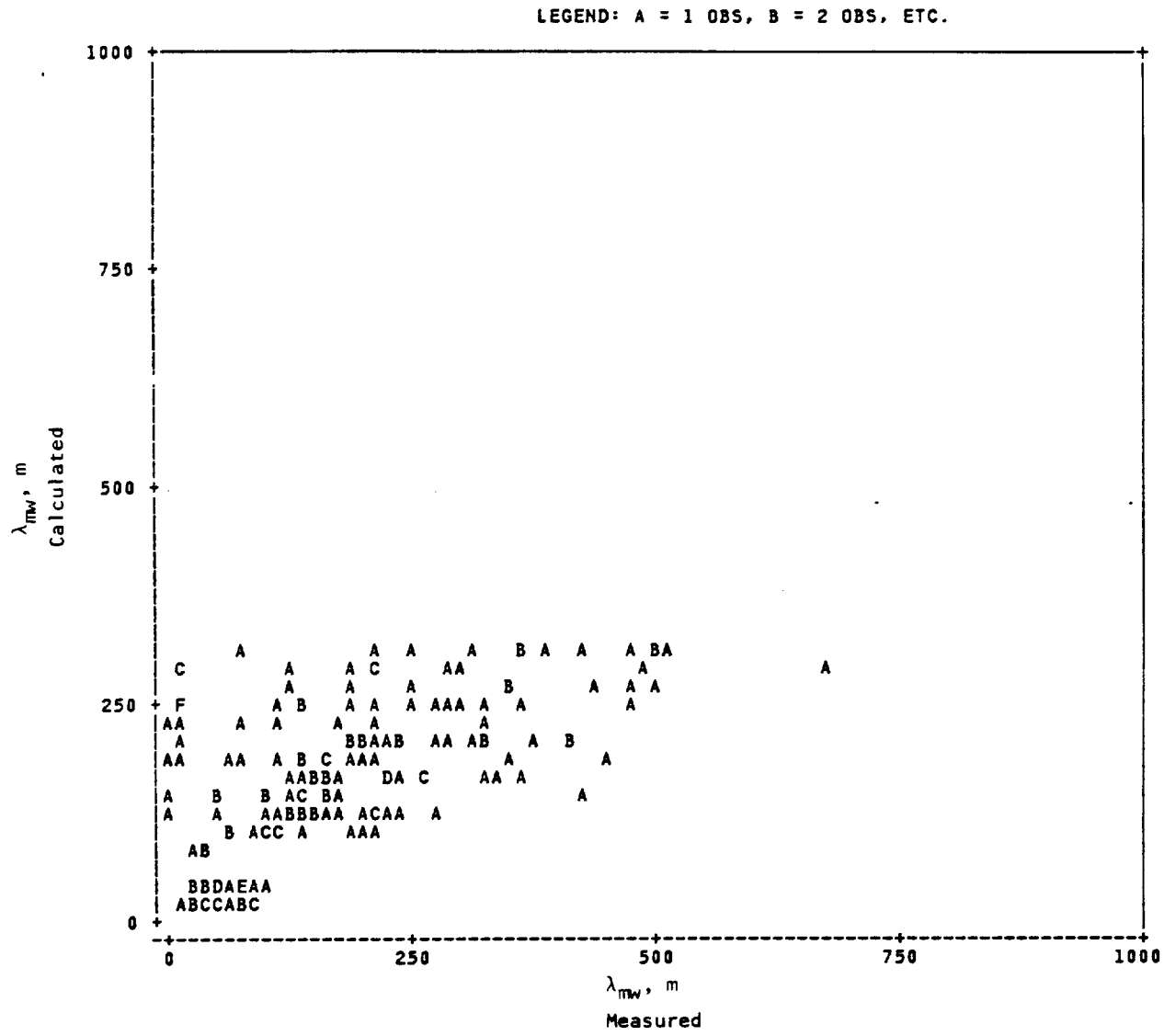

FIGURE 15. λ_{mw} computed from Equations 24 and 19 using Gill propeller measurements vs. λ_{mw} from measurements at six tower levels using cups and bivanes.

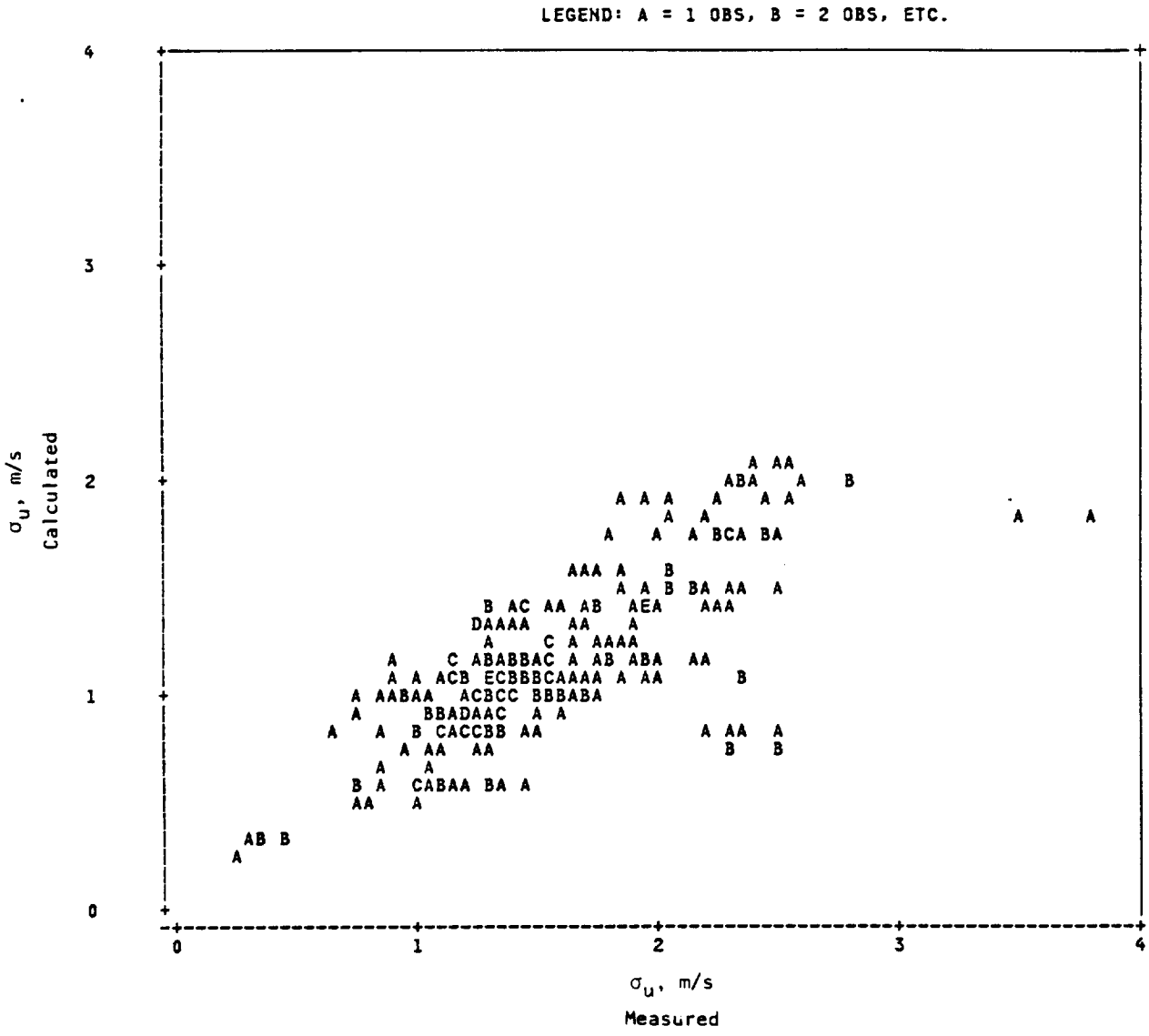

FIGURE 16. σ_u computed from Equation 28 using Gill propeller measurements vs. σ_u from measurements at six tower levels using cups and bivanes.

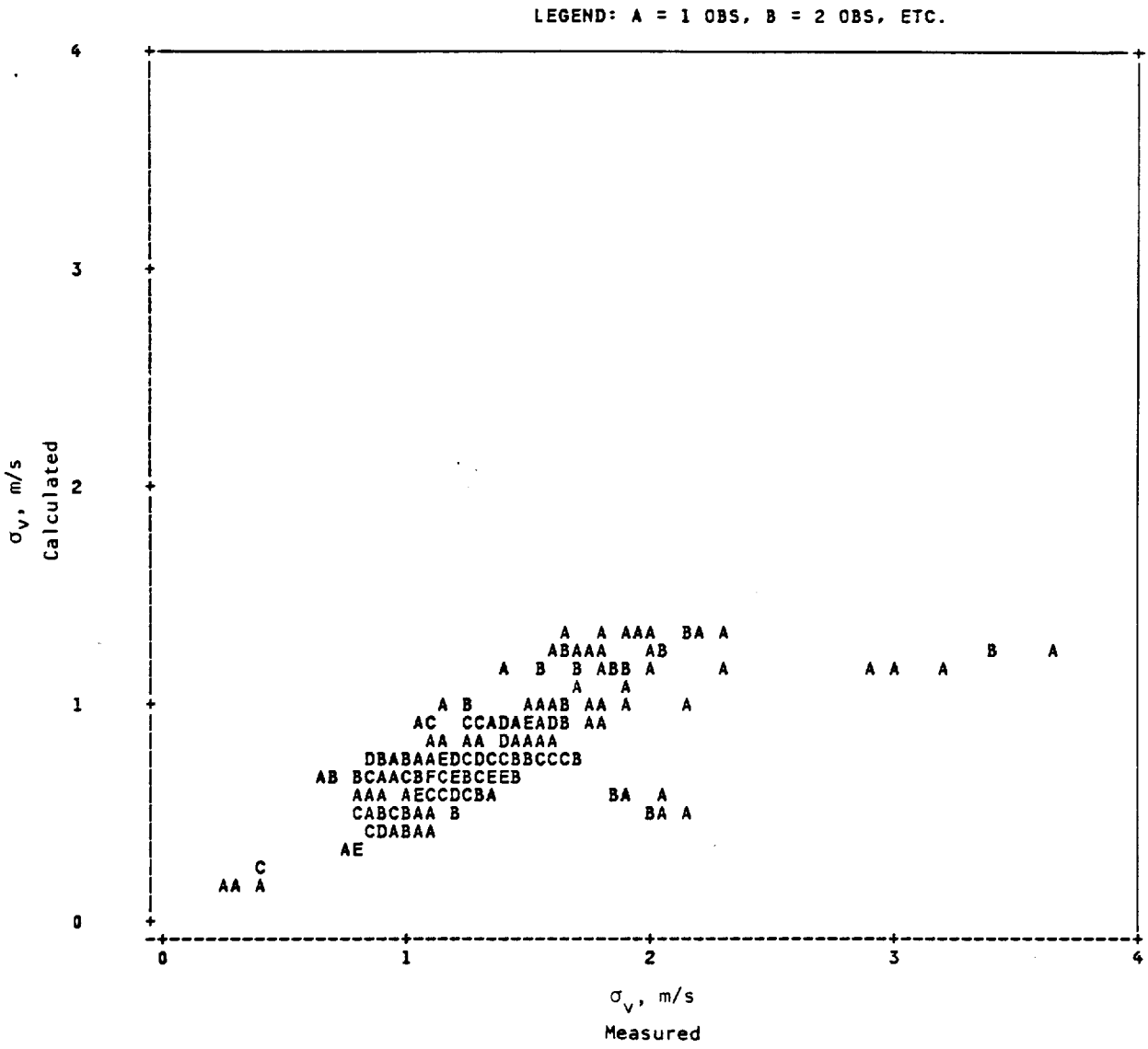

FIGURE 17. σ_v computed from Equation 29 using Gill propeller measurements vs. σ_v from measurements at six tower levels using cups and bivanes.

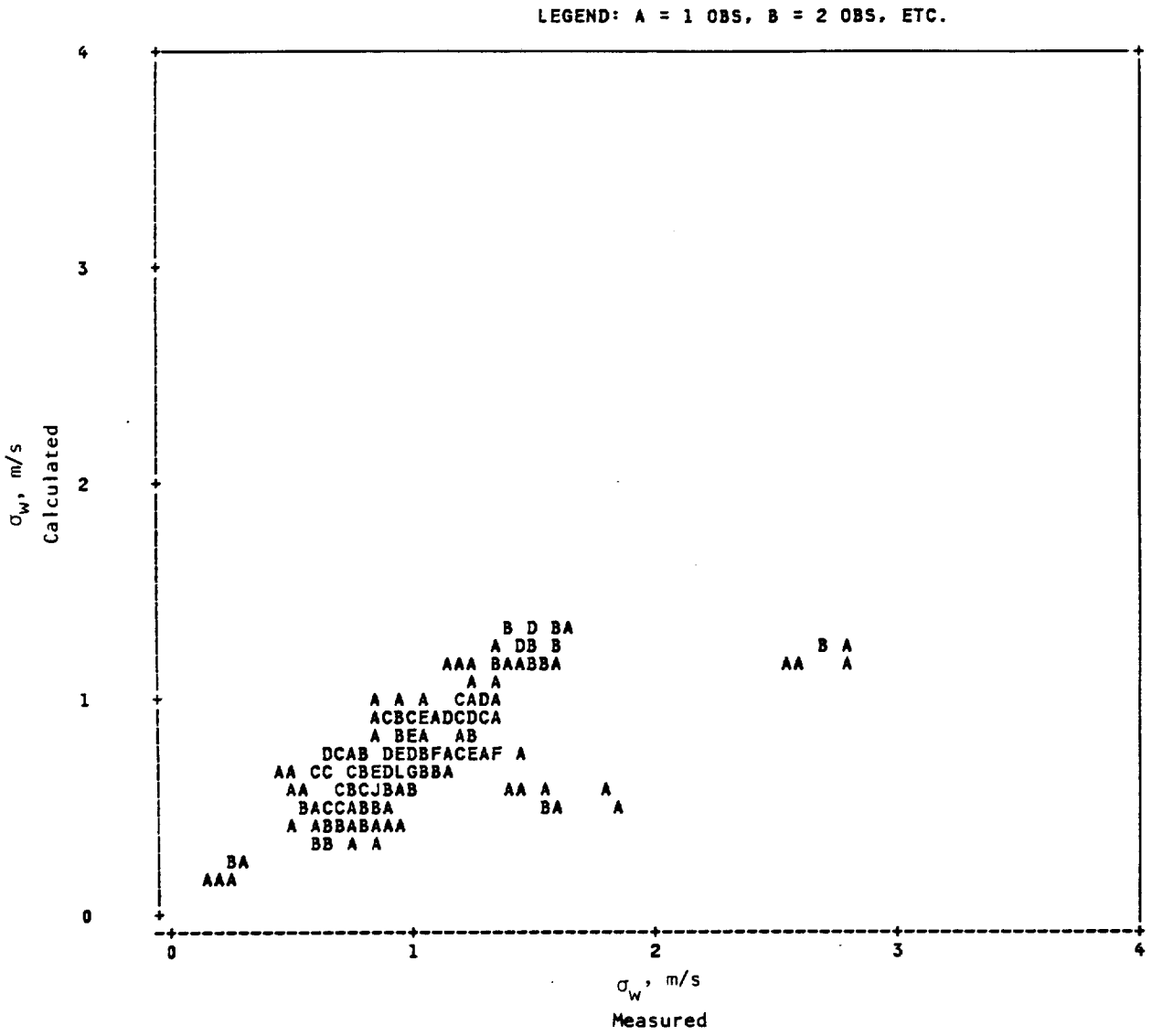

FIGURE 18. σ_w computed from Equation 29 using Gill propeller measurements vs. σ_w from measurements at six tower levels using cups and bivanes.

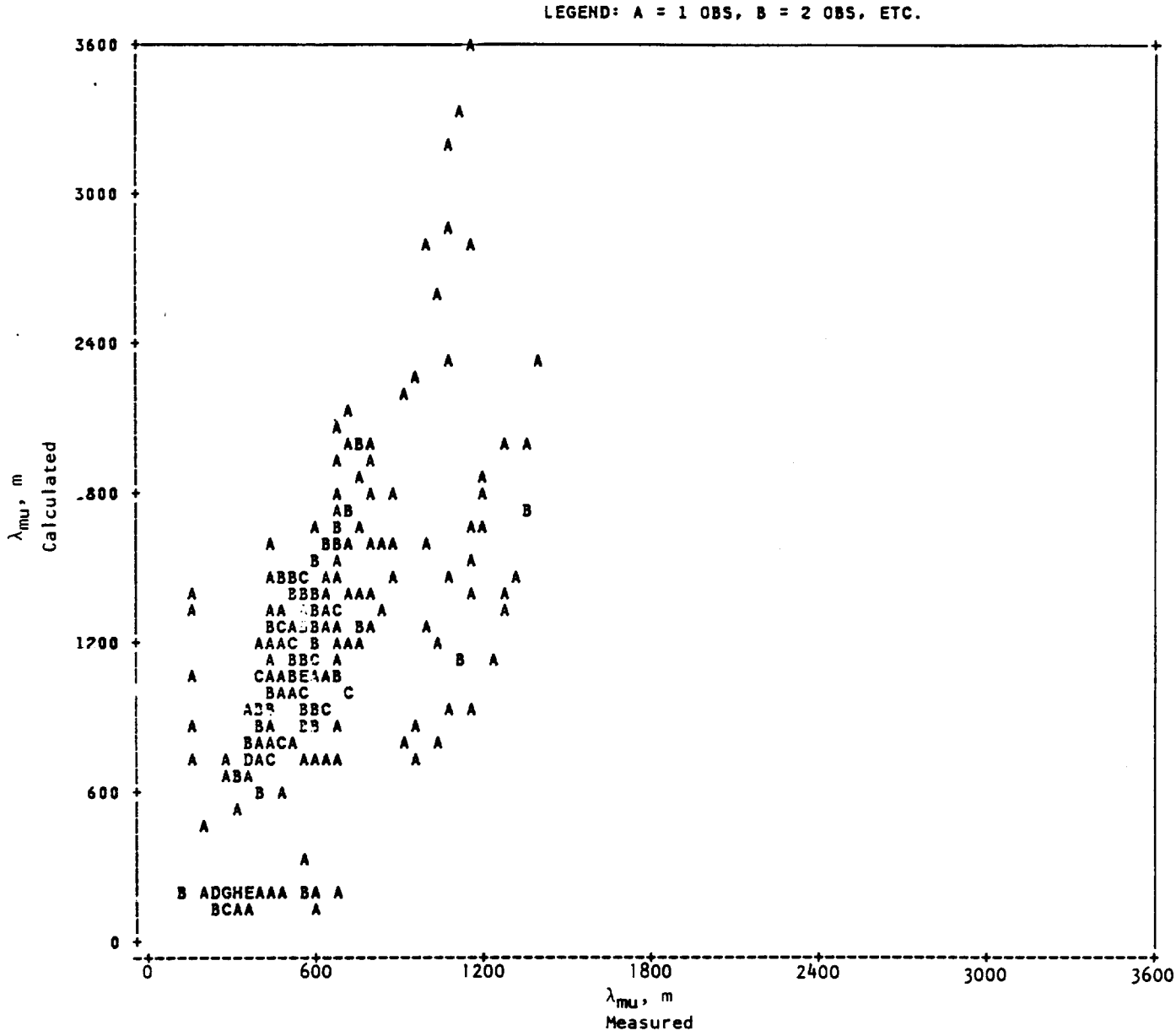

FIGURE 19. λ_{mu} computed from Equations 30 and 8b using Gill propeller measurements vs. λ_{mu} from measurements at six tower levels using cups and bivanes.

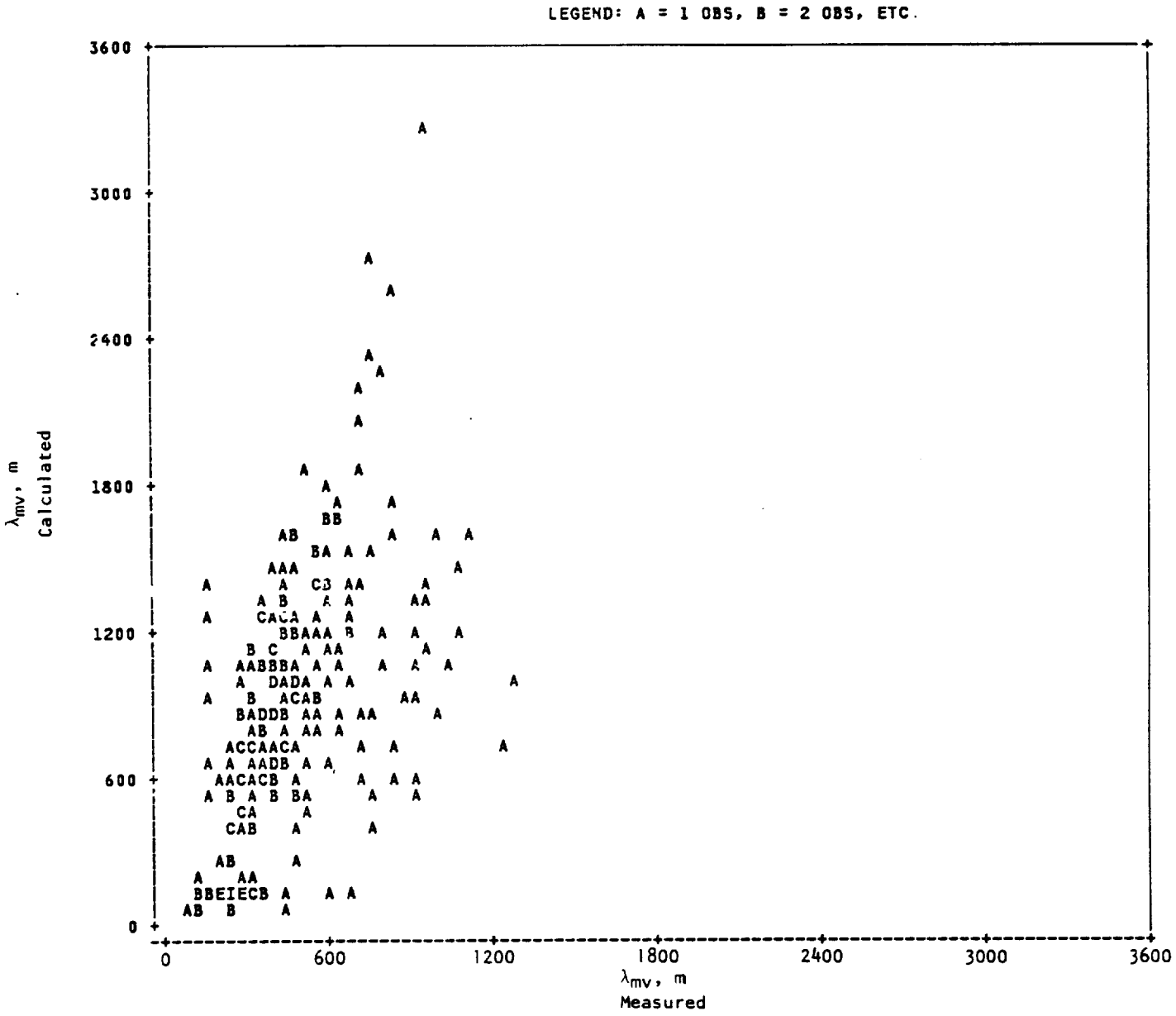

FIGURE 20. λ_{mv} computed from Equation 30 and 8b using Gill propeller measurements vs. λ_{mv} from measurements at six tower levels using cups and bivanes.

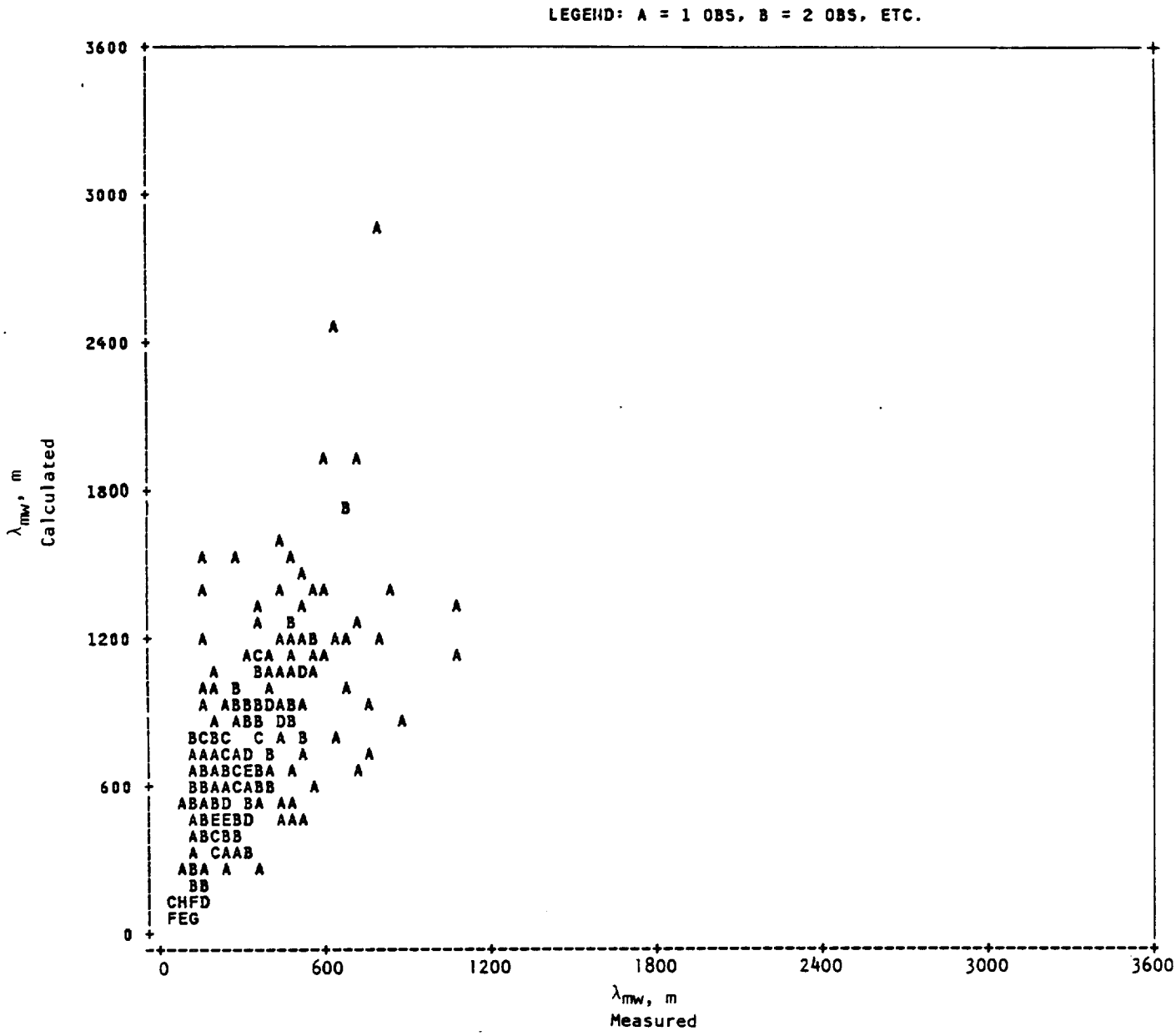

FIGURE 21. λ_{mw} computed from Equations 30 and 8b using Gill propeller measurements vs. λ_{mw} from measurements at six tower levels using cups and bivanes.